JOURNAL OF PETROLOGY

Journal of Petrology, 2017, Vol. 58, No. 12, 2403–2428
doi: 10.1093/petrology/egy016
Advance Access Publication Date: 27 February 2018
Original Article

OXFORD

Deep-seated Carbonatite Intrusion and Metasomatism in the UHP Tromsø Nappe, Northern Scandinavian Caledonides—a Natural Example of Generation of Carbonatite from Carbonated Eclogite

Erling K. Ravna[1]*, Dmitry Zozulya[2], Kåre Kullerud[1,3], Fernando Corfu[4], Peter I. Nabelek[5], Marian Janák[6], Trond Slagstad[7], Børre Davidsen[7], Rune S. Selbekk[8] and Hans-Peter Schertl[9,10]

[1]Department of GeoSciences, UiT/The Arctic University of Norway, N-9037 Tromsø, Norway; [2]Geological Institute, Kola Scientific Center, Russian Academy of Sciences, Apatity 184209, Russia; [3]Norwegian Mining Museum, N-3616 Kongsberg, Norway; [4]Department of Geosciences, University of Oslo and CEED, N-0315 Oslo, Norway; [5]Department of Geological Sciences, University of Missouri, Columbia, MO 65211, USA; [6]Earth Science Institute, Slovak Academy of Sciences, Bratislava, Slovak Republic; [7]Geological Survey of Norway, N-7491 Trondheim, Norway; [8]Natural History Museum, University of Oslo, N-0315 Oslo, Norway; [9]Institute of Geology, Mineralogy and Geophysics, Ruhr-University Bochum, 44801 Bochum, Germany; [10]College of Earth Science & Engineering, Shandong University of Science and Technology, Qingdao 266590, China

*Corresponding author. E-mail: erling.ravna@uit.no

Received September 20, 2016; Accepted February 12, 2018

ABSTRACT

Carbonatites (*sensu stricto*) are igneous rocks typically associated with continental rifts, being emplaced at relatively shallow crustal levels or as extrusive rocks. Some carbonatites are, however, related to subduction and lithospheric collision zones, but so far no carbonatite has been reported from ultrahigh-pressure (UHP) metamorphic terranes. In this study, we present detailed petrological and geochemical data on carbonatites from the Tromsø Nappe—a UHP metamorphic terrane in the Scandinavian Caledonides. Massive to weakly foliated silicate-rich carbonate rocks, comprising the high-*P* mineral assemblage of Mg–Fe-calcite ± Fe-dolomite + garnet + omphacitic clinopyroxene + phlogopite + apatite + rutile + ilmenite, are inferred to be carbonatites. They show apparent intrusive relationships to eclogite, garnet pyroxenite, garnet–mica gneiss, foliated calc-silicate marble and massive marble. Large grains of omphacitic pyroxene and megacrysts (up to 5 cm across) of Cr-diopside in the carbonatite contain rods of phlogopite oriented parallel to the *c*-axis, the density of rods being highest in the central part of the megacrysts. Garnet contains numerous inclusions of all the other phases of the carbonatite, and, in places, composite polyphase inclusions. Zircon, monazite and allanite are common accessory phases. Locally, veins of silicate-poor carbonatite (up to 10 cm across) occur. Extensive fenitization by K-rich fluids, with enrichment in phlogopite along contacts between carbonatite and silicate country rocks, is common. Primitive mantle-normalized incompatible element patterns for the carbonatite document a strong enrichment of light rare earth elements, Ba and Rb, and negative anomalies in Th, Nb, Ta, Zr and Hf. The carbon and oxygen isotope compositions of the carbonatite are distinctly different from those of the spatially associated calc-silicate marble, but also from mantle-derived carbonatites elsewhere. Neodymium and Sr isotope data coupled with the trace element distribution indicate a similarity of the Tromsø carbonatite to orogenic (off-craton) carbonatites rather than to anorogenic (on-craton) ones. U–Pb dating of relatively U-rich prismatic, oscillatory-zoned zircon gives an age of 454·5 ± 1·1 Ma. We suggest that

the primary carbonatite magma resulted from partial melting of a carbonated eclogite at UHP, in a deeply subducted continental slab.

Key words: carbonatite; ultrahigh-pressure melting; carbonated eclogite; subduction zone; metasomatism

INTRODUCTION

The occurrence of carbonate-rich rocks in high- to ultrahigh-pressure (HP to UHP) terranes has attracted increased attention from various research groups (e.g. Schertl & Okay, 1994; Ogasawara *et al.*, 2002; Korsakov & Hermann, 2006; Liu *et al.*, 2006; Castelli *et al.*, 2007; Proyer *et al.*, 2008; Ferrando *et al.*, 2011; Massonne, 2011; Proyer *et al.*, 2011*a*, 2011*b*). Korsakov & Hermann (2006) reported on silicate and carbonate melt inclusions associated with diamonds in garnet and clinopyroxene from UHP carbonate rocks. They concluded that this represented the first direct evidence for carbonate melts in deeply subducted crust. Liu *et al.* (2006) described carbonatite-like dykes from the eastern Himalayan syntaxis, and concluded that they were a result of melting of metasedimentary carbonate rocks within the orogenic crust. None of these rocks in HP or UHP terranes seems to have affinity to mantle-derived carbonatites. Carbonatites (*sensu stricto*) are igneous rocks containing >50 modal % carbonate minerals, and therefore they resemble marbles. They are typically associated with continental rifts (e.g. the East African Rift Zone; Le Bas, 1987) and are emplaced at relatively shallow crustal levels or as extrusive rocks (e.g. Oldoinyo Lengai; Bailey, 1989). However, some carbonatites are related to subduction and lithospheric collision zones (Le Bas *et al.*, 1987; Tilton *et al.*, 1998; Hou *et al.*, 2006; D'Orazio *et al.*, 2007; Chakhmouradian *et al.*, 2008; Sklyarov *et al.*, 2009). Identification of carbonatites is often hampered by nearby presence of marbles of sedimentary origin (Sklyarov *et al.*, 2009). As far as we are aware, no carbonatite has hitherto been reported from HP or UHP metamorphic terranes, although carbonatite melt inclusions in garnet and clinopyroxene have been described in diamond-facies metasedimentary rocks from the Kokchetav Massif in Kazakhstan (Korsakov & Hermann, 2006). As carbonatite melts are extremely reactive (e.g. Green & Wallace, 1988), they are expected to be at least partly consumed by interaction with subducted country rocks or mantle peridotite.

This study reports on the occurrence, petrography, age and geochemistry of carbonatite found within UHP metamorphic rocks (eclogite, garnet pyroxenite, diamond-bearing gneiss and marbles) of the Tromsø Nappe, the uppermost tectonic unit of the northern Scandinavian Caledonides (Fig. 1). It is proposed that carbonatite resulted from partial melting of carbonated eclogite in deeply subducted continental crust at UHP conditions.

GEOLOGICAL SETTING

The Tromsø Nappe of the uppermost allochthon of the northern Scandinavian Caledonides consists of a metasedimentary sequence with bodies of mafic to ultramafic rocks. Roberts & Gee (1985) suggested that this unit represents an exotic continental fragment of Laurentian affinity as it appears above a tectonic unit of oceanic (Iapetus) rocks that mark the suture zone between Baltica and Laurentia. Janák *et al.* (2012) suggested that the Tromsø Nappe belonged to the outermost continental margin of Baltica, which had already been subducted before the terminal Scandian collision, and was emplaced as an out-of-sequence thrust during the Scandian lateral transport of nappes. However, the paleogeographical status of the Tromsø Nappe is still not understood.

Marble, calc-silicate marble and garnet–mica gneiss, hosting numerous eclogite bodies and a few occurrences of garnet-bearing ultramafic rocks (Ravna *et al.*, 2006), dominate the metasedimentary sequence. Maximum *P*–*T* conditions are estimated at *c.* 3·3–3·5 GPa, ~750°C (Ravna & Roux, 2006; Janák *et al.*, 2012, 2013, 2015). Janák *et al.* (2013) also discovered microdiamonds in a garnet–mica gneiss. Stevenson (2005) was able to establish two post-peak-*P* partial melting events in eclogites: one at 2·0–2·2 GPa with peritectic garnet and the second at 1·0–1·3 GPa with peritectic hornblende.

Corfu *et al.* (2003) carried out U–Pb zircon and titanite age dating of the eclogitic rocks of the Tromsø Nappe. Primary magmatic zircon from a garnet–omphacite-bearing trondhjemite gneiss layer within the Tromsdalstind eclogite (Krogh *et al.* 1990) yielded an age of 493 Ma (Corfu *et al.*, 2003), which was interpreted as the intrusion age of the protolith. A low-Al titanite in a post-eclogite hornblende-bearing leucosome gave an age of 450·3 ± 0·9 Ma, whereas a large rutile porphyroblast gave 448·8 ± 1·4 Ma. Timing of the UHP eclogite formation is constrained by a 452·1 ± 1·7 Ma age of zircon from the Tønsvika eclogite. Slightly younger ages of 451–450 Ma were provided by high-Al titanite from eclogite and calc-silicate rock. Rutile fragments from the Tønsvika eclogite gave an age of 428·4 ± 0·8 Ma (Corfu *et al.*, 2003).

FIELD RELATIONS

The carbonatite crops out along the shore at two localities about 1 km apart on both sides of a small bay that hosts the delta of the river Tønsvikelva, just to the NE of

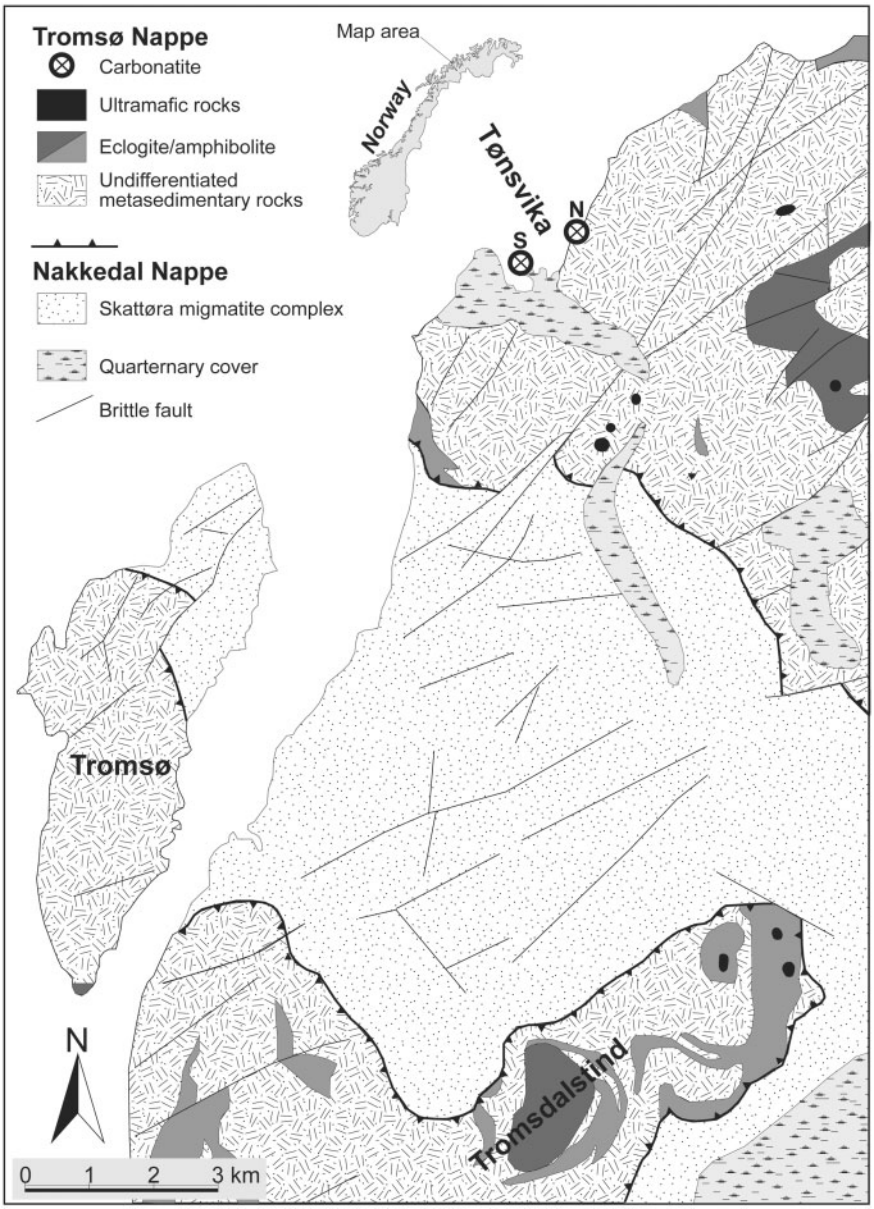

Fig. 1. Geological setting of the Tromsø carbonatites. S and N denote southern and northern exposures of carbonatite, respectively.

Tromsø (Fig. 1). A detailed map of the shore exposure at locality Tønsvika S is shown in Fig. 2.

The carbonatite is associated with eclogite and its retrograde products, Cr-rich garnet clinopyroxenite and glimmerite, marbles, calc-silicate marble and garnet–mica gneiss. Carbonatite is interlayered with and penetrates the country rocks as veins and small dikes (Fig. 3a and b). It has cut across the UHP fabric of adjacent eclogite and has caused local metasomatism with growth of phlogopite in the eclogite and Cr-rich (locally garnet-bearing) clinopyroxenite (Fig. 3b, e and m).

Carbonatite also cuts across marble (Fig. 3f). The calc-silicate marble is strongly foliated and folded, and locally contains trails of numerous small pods and lenses of retrogressed eclogite (Fig. 3h). Along the contact between retrograde eclogite and the marble, a thin ($<$1 cm) dark zone of hydration (amphibolitization) is developed (Fig. 3h), but there is no evidence of K-metasomatism, as can be seen along the carbonatite–eclogite boundaries.

The carbonatite generally has a coarse-grained isotropic fabric with clusters of mafic silicates (mainly garnet, biotite and clinopyroxene) evenly distributed in the carbonate matrix, suggesting that it is igneous (Fig. 3i and j). There are also local patches and veins of pure carbonatite (Fig. 3g and l). Megacrysts of Cr-diopside, which are up to 5 cm across (Fig. 3k), occur sporadically. A metasomatic alteration zone of phlogopite-bearing clinopyroxenite grading into glimmerite is locally developed along the contact between carbonatite and eclogite or Cr-rich garnet clinopyroxenite, with a consequent depletion of K in the carbonatite.

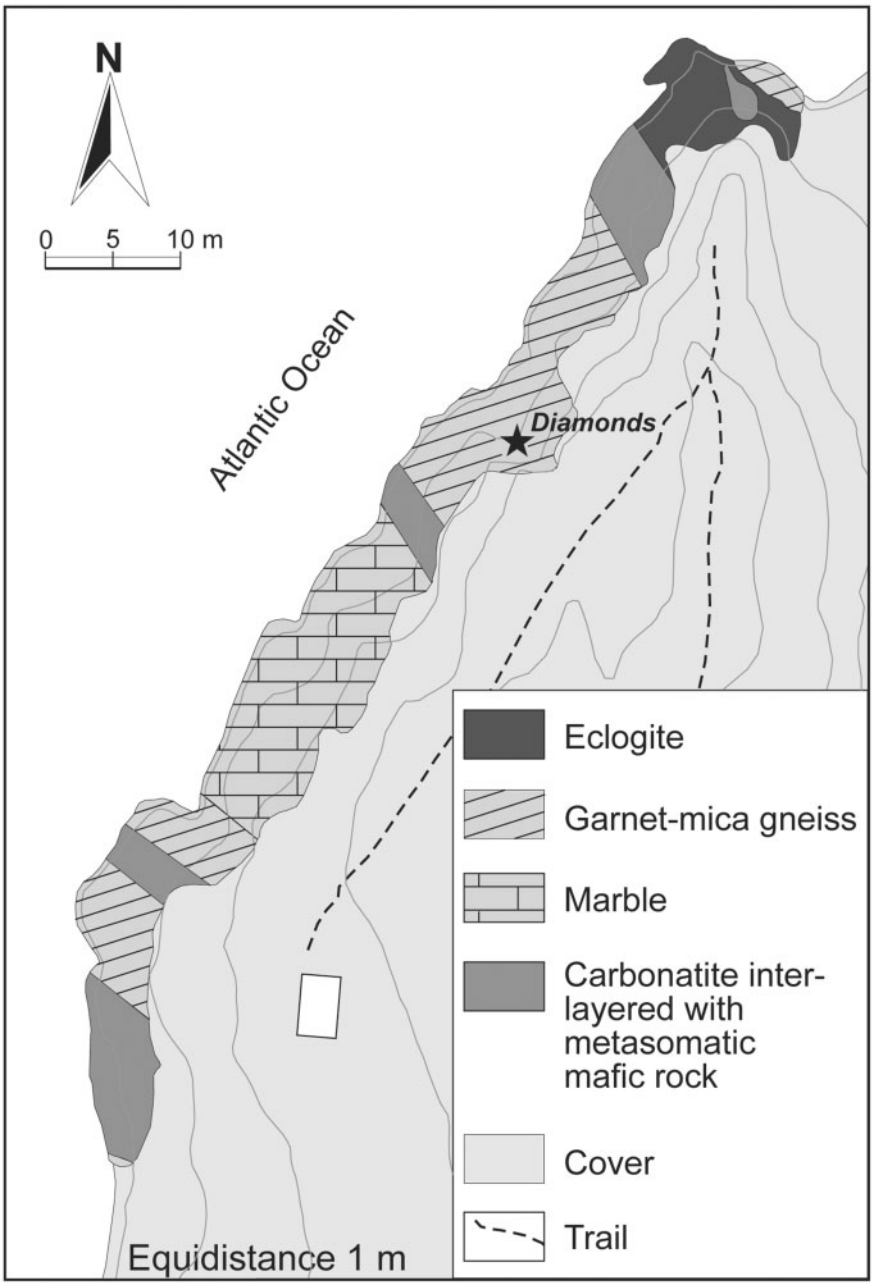

Fig. 2. Detailed map of the shore exposures at the southern locality.

ANALYTICAL METHODS

Mineral analyses

Mineral abbreviations used throughout the paper are after Kretz (1983), except for the terms Cats (calcium-Tschermak's molecule) and Quad [quadrilateral (Ca–Mg–Fe) pyroxenes] (see Morimoto *et al.*, 1989). Most of the chemical compositions of minerals were determined by a CAMECA SX-100 electron microprobe at the State Geological Institute of Dionýz Štúr in Bratislava. The operating conditions were 15 kV accelerating voltage, 20 nA beam current, counting times 20 s on-peak counting times and beam diameter of 2 –10 μm. Mineral standards (Si, Ca: wollastonite; Na: albite; K: orthoclase; Fe: fayalite; Mn: rhodonite), pure synthetic element oxides (TiO_2, Al_2O_3, Cr_2O_3, MgO) and Ni metal were used for calibration. Raw counts were corrected using the PAP routine.

Some samples were analyzed ny energy-dispersive spectrometry (EDS) on a JEOL JSM-6300 scanning electron microscope (SEM) at The Arctic University of Norway, Tromsø, using ZAF matrix correction and optimized EDAX SEC-factors based on the use of mineral standards [Ca, Si: wollastonite; Na, Al: jadeite (Jd_{100}; Clear Creek; Coleman, 1961); K: orthoclase; Fe: fayalite; Mg: diopside; Mn: rhodonite] and pure synthetic oxides (TiO_2, Cr_2O_3). Totals of these analyses are normalized to

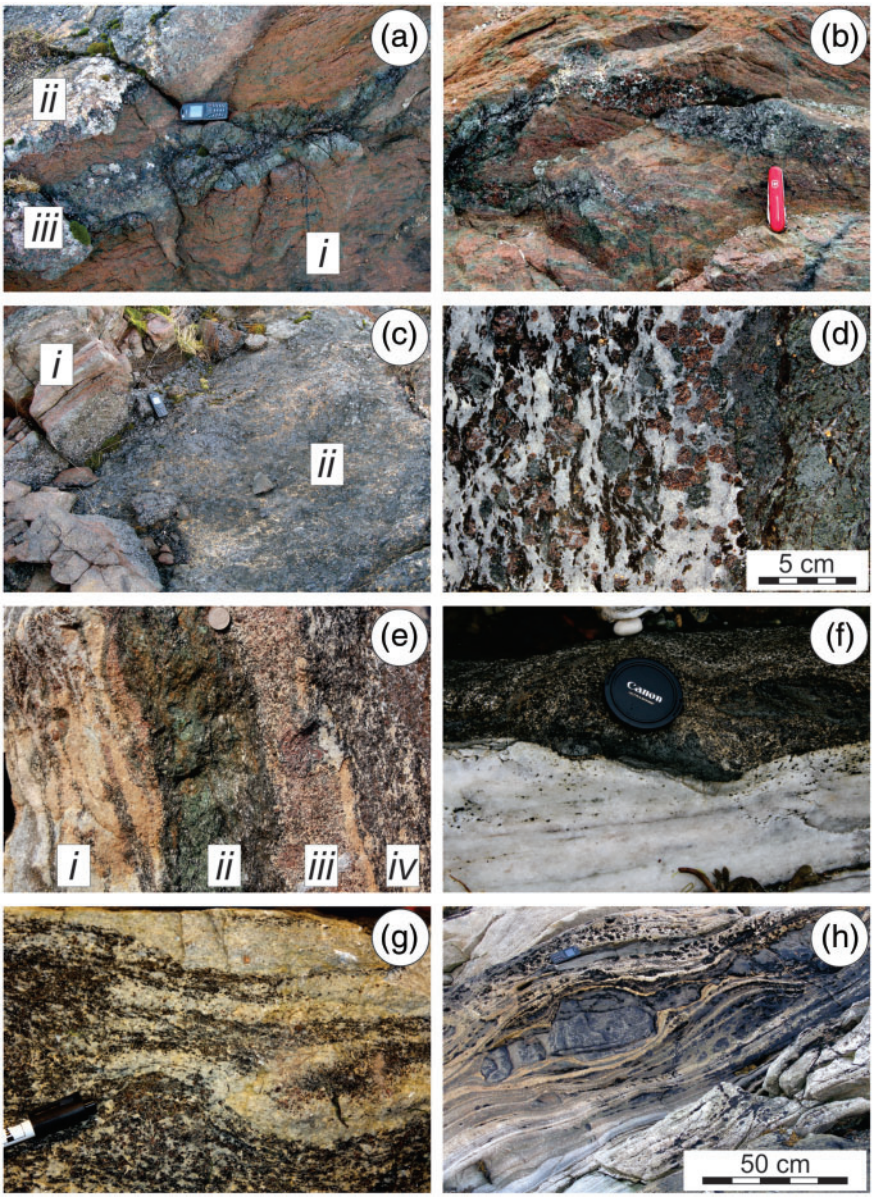

Fig. 3. Field relations and rock types. (a) Contact between eclogite (*i*) and C1 carbonatite (*ii*). A metasomatic alteration zone occurs along the contact (*iii*). (b) Carbonate-rich vein with metasomatic alteration zone cross-cutting eclogite fabrics. (c) Eclogite (*i*) apparently intruded by C1 carbonatite (*ii*). (d) Detail of contact between C1 carbonatite and metasomatized eclogite. (e) Relationship between garnet-bearing Cr-rich clinopyroxenite (*ii*) and various types of carbonatite: (*i*) silica-poor C2; (*iii*) garnet-rich C1; (*iv*) garnet–phlogopite-rich C1. (f) Sharp contact between common marble (white) and C1 carbonatite. (g) Schlieren of C2 carbonatite in Grt–Cpx–Phl-rich C1 carbonatite. (h) Boudins of eclogite in marble. There are no signs of metasomatic reactions between these rocks. (i) Massive C1 carbonatite with garnet, phlogopite and omphacite in calcitic matrix. (j) Massive phlogopite-poor C1 carbonatite with garnet evenly distributed in calcitic matrix. (k) Megacryst (5 cm across) of Cr-rich diopside in C1 carbonatite. (l) Vein of C2 carbonatite in C1 carbonatite. (m) Cr-rich Grt-pyroxenite. (n) Detail of Cr-diopside-bearing glimmerite positioned between carbonatite and pyroxenite.

100 wt %. Area scans across clinopyroxenes with lamellae of phlogopite were also carried out on this equipment.

Fragments (~2 g) of clinopyroxene megacrysts with rods of phlogopite from carbonatite and pyroxenite were carefully handpicked for bulk X-ray fluorescence (XRF) analysis, using analytical procedures that are described below for major and minor element analysis of bulk-rock.

Representative analyses of clinopyroxene, garnet, phlogopite and carbonates are given in Tables 1–4.

Bulk-rock analysis

Major, minor and trace element data for carbonatite, calc-silicate marble, eclogite, retrogressed eclogite, metasomatic eclogite, pyroxenite and glimmerite were obtained at the Norwegian Geological Survey (NGU),

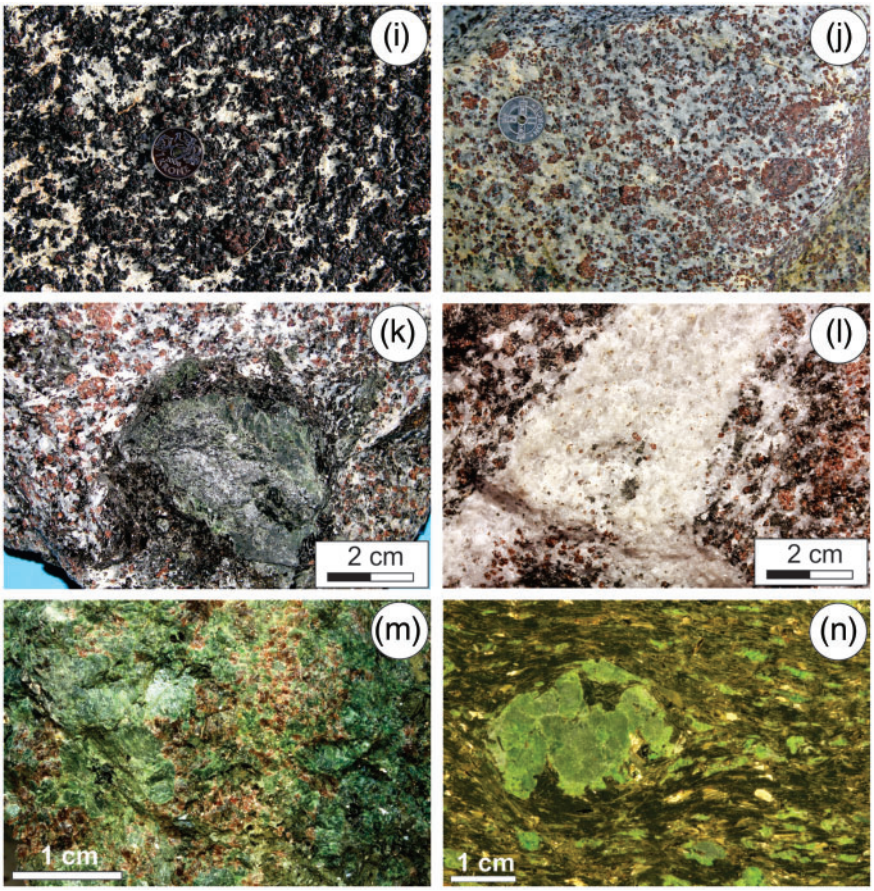

Fig. 3. Continued.

Table 1: Representative clinopyroxene compositions

Rock:	C1					Pxite				ME	Eclogite	Marble
Sample:	T4/07B		TN-T4A1			TN-T3	TN-T1/07			TN	TN-T5	TN-T1-05
	matrix*	light lam	matrix*	megaX*	megaX†	matrix*	matrix†	matrix*	scan matrix‡	matrix‡	matrix‡	matrix‡
SiO_2	52·8	52·6	53·5	53·8	52·4	54·0	54·0	54·7	54·5	54·0	54·8	52·8
Al_2O_3	4·28	3·77	3·95	2·69	3·96	4·73	1·47	1·29	1·99	3·45	9·67	9·97
TiO_2	0·23	0·20	0·13	0·06	0·19	0·12	0·10	0·03	0·09	0·08	0·24	n.d.
Cr_2O_3	n.d.	0·03	n.d.	0·32	0·24	0·21	0·38	0·44	0·40	n.d.	n.d.	n.d.
FeO	11·4	14·0	6·42	4·52	4·87	4·12	3·50	3·09	3·14	3·38	4·77	5·68
MnO	0·06	0·10	0·03	0·05	0·10	0·03	0·11	0·10	n.d.	0·08	n.d.	n.d
MgO	9·85	10·83	12·8	14·3	16·1	13·6	17·7	16·1	16·9	15·1	9·43	9·41
CaO	18·9	17·5	21·1	22·3	20·0	21·7	21·3	23·2	21·7	22·1	15·9	18·7
Na_2O	2·99	2·42	1·94	1·45	1·03	1·98	0·80	0·89	1·14	1·80	5·19	3·46
K_2O	n.d.	n.d.	n.d.	n.d.	0·55	n.d.	0·31	n.d.	0·26	n.d.	n.d.	n.d.
Total	100·6	101·5	99·9	99·5	99·5	100·5	99·4	99·8	100·0	100·0	100·0	100·0
6 oxygen												
Si	1·97	1·96	1·97	1·98	1·93	1·96	1·97	1·99	1·98	1·96	1·97	1·92
Al_{tot}	0·19	0·17	0·17	0·12	0·17	0·20	0·06	0·06	0·09	0·15	0·41	0·43
Ti	0·01	0·01	—	—	0·01	—	—	—	—	—	—	—
Cr	—	—	—	0·01	0·01	0·01	0·01	0·01	0·01	—	—	—
Fe_{tot}	0·36	0·44	0·20	0·14	0·15	0·13	0·11	0·09	0·10	0·10	0·14	0·17
Mn	—	—	—	—	—	—	—	—	—	—	—	—
Mg	0·55	0·60	0·70	0·78	0·88	0·73	0·96	0·88	0·91	0·82	0·50	0·51
Ca	0·76	0·70	0·83	0·88	0·79	0·84	0·83	0·91	0·84	0·86	0·61	0·73
Na	0·22	0·17	0·14	0·10	0·07	0·14	0·06	0·06	0·08	0·13	0·36	0·24
K	—	—	—	—	0·03	—	0·01	—	0·01			
Total	4·04	4·04	4·01	4·01	4·03	4·01	4·03	4·00	4·02	4·03	4·00	3·99
Mg#	60·6	58·0	78·0	84·9	85·5	85·5	90·0	90·3	90·6	88·8	77·9	74·7

C1, carbonatite type 1; Pxite, pyroxenite; ME, metasomatized eclogite; megaX, megacryst; lam, lamella.
*WDS Bratislava.
†XRF bulk sample, Tromsø.
‡EDS Tromsø.

Table 2: Representative garnet compositions

Rock:	C1*		C2*	Pxite*	ME†	Eclogite†	Marble†
Sample:	T4/07	TN-T4A	TN-T1/08	TN-T3/08	TN-5	TN-T5	TN-T1-05
SiO_2	38·0	38·9	39·1	40·2	40·6	39·0	39·4
Al_2O_3	20·3	21·5	20·9	22·3	22·5	21·8	22·1
TiO_2	0·15	0·10	0·19	0·05	0·07	0·09	n.d.
Cr_2O_3	0·02	0·19	n.d.	0·26	n.d.	0·07	n.d.
FeO	26·1	21·0	20·9	18·6	15·9	22·1	14·2
MnO	0·70	0·43	0·90	0·44	0·71	0·56	0·32
MgO	4·26	6·82	5·26	10·0	13·5	6·33	3·47
CaO	10·7	11·0	12·3	9·14	6·84	10·1	20·5
Na_2O	0·02	n.d.	0·03	0·03	n.d.	n.d.	n.d.
Total	100·3	99·9	99·6	101·1	100·0	100·0	100·0
12 oxygen							
Si	2·99	2·99	3·03	3·00	3·00	3·00	3·01
Al_{tot}	1·88	1·95	1·91	1·96	1·96	1·98	1·99
Ti	0·01	0·01	0·01	—	—	0·01	—
Cr	—	0·01	n.d.	0·02	—	—	—
Fe_{tot}	1·72	1·35	1·36	1·16	0·98	1·42	0·91
Mn	0·05	0·03	0·06	0·03	0·04	0·04	0·02
Mg	0·50	0·78	0·61	1·11	1·49	0·73	0·40
Ca	0·90	0·91	1·02	0·73	0·54	0·83	1·68
Na	—	—	0·01	—	—	—	—
Total	8·06	8·02	8·01	8·01	8·02	8·00	8·00
X_{Ca}^{Grt}	0·285	0·296	0·336	0·241	0·177	0·276	0·559
Mg#	22·5	36·7	30·9	48·9	60·2	33·8	30·3

ME, metasomatized eclogite.
*WDS Bratislava.
†EDS Tromsø.

Table 3: Representative mica compositions

Rock:	C1				C2	Pxite	
Sample:	TN-T4A		TN-T4/07B		TN-1-08	TN-T1/07	
Mineral:	Phl* matrix	Phl* lam	Phl1 lam	Phl1 matrix	Phl1 matrix	Phl1 matrix	Phl1 lam
SiO_2	37·7	39·4	36·6	37·1	37·7	40·9	40·9
Al_2O_3	16·7	15·7	14·3	14·8	16·6	13·9	13·9
TiO_2	2·98	1·68	4·23	3·77	2·87	1·38	1·19
Cr_2O_3	0·10	0·34	—	—	—	0·60	0·68
FeO	12·0	8·45	19·6	17·4	13·6	5·51	5·15
MnO	0·01	0·03	0·03	0·03	0·03	n.d.	n.d.
MgO	15·3	19·4	10·5	12·4	14·38	22·1	22·4
CaO	0·10	0·22	0·20	0·01	0·02	0·21	0·01
Na_2O	0·30	0·20	0·09	0·20	0·21	0·12	0·17
K_2O	9·31	9·38	9·22	9·28	9·10	9·90	9·99
Total	94·5	94·7	94·8	94·9	94·5	94·6	94·4
O	11	11	11	11	11	11	11
Si	2·79	2·85	2·82	2·81	2·80	2·93	2·94
Al_{tot}	1·46	1·34	1·30	1·32	1·46	1·18	1·18
Ti	0·17	0·09	0·25	0·22	0·16	0·07	0·06
Cr	0·01	0·02	—	—	—	0·03	0·04
Fe_{tot}	0·74	0·51	1·26	1·10	0·85	0·33	0·31
Mn	—	—	—	—	—	—	—
Mg	1·69	2·09	1·20	1·40	1·60	2·36	2·40
Ca	0·01	0·02	0·02	—	—	0·02	—
Na	0·04	0·03	0·01	0·03	0·03	0·02	0·02
K	0·88	0·87	0·90	0·90	0·86	0·91	0·92
Total	7·78	7·82	7·75	7·78	7·76	7·85	7·86
Mg#	69·4	80·4	48·7	55·9	65·4	87·7	88·6

lam, lamellae or rod in cpx.

Trondheim and the Department of Geosciences, UiT/The Arctic University of Norway (IG-UiT). Major and minor elements were analyzed on fused $Li_2B_4O_7$ glass beads by wavelength-dispersive XRF spectrometry (PANalytical Axios at NGU and Bruker Tiger SX8 at IG-UiT). Trace elements were analyzed by XRF spectrometry on pressed powder pellets at NGU and IG-UiT, and by laser ablation inductively coupled plasma mass

spectrometry (LA-ICP-MS) on fused glass beads using a Finnigan MAT Element 1 at NGU. The CO_2 content of selected samples of carbonatite and calc-silicate marble was analyzed on a LECO CS 200 at IG-UiT and by titration (volumetric analysis) at the Geological Institute, Kola Science Center in Apatity, Russia. Concentrations of F were determined at the Geological Institute, Kola Science Centre using ion-selective electrode (ISE) potentiometry [for a description of the method, see Cazes (2005)].

Major and minor element compositions of selected samples are presented in Table 5, and trace elements in Table 6. Additional data are available from the Supplementary Data Table S1; supplementary data are available for downloading at http://www.petrology.oxfordjournals.org.

Carbon and oxygen isotope compositions of carbonatite and calc-silicate marble were analyzed by a dual-inlet Delta Plus mass spectrometer using a Kiel device for acid dissolution of carbonates at the University of Missouri, Columbia. Reproducibility is better than 0·1‰ for both C and O. Results are given in Table 7.

Whole-rock samples of carbonatites and related rocks were analyzed for Sm–Nd and Rb–Sr isotopes in the laboratory of geochronology and isotope geochemistry of the Geological Institute of the Kola Science Center, Apatity. Nd isotopes and Sm and Nd concentrations were determined by isotope dilution and measurements on a Finnigan MAT 262 (RPQ) multicollector mass spectrometer in a static mode using Ta + Re filaments. The measured reproducibility for eight parallel Nd-isotope analyses of the La Jolla standard ($^{143}Nd/^{144}Nd = 0.511833 \pm 6$) was 0·0024% (2σ). Eight $^{147}Sm/^{144}Nd$ measurements of the BCR standard yielded an average error of 0·2% (2σ). Laboratory blanks for Nd and Sm are 0·3 and 0·06 ng, respectively. All $^{143}Nd/^{144}Nd$ ratios were normalized to $^{146}Nd/^{144}Nd = 0.7219$ and corrected using $^{143}Nd/^{144}Nd = 0.511860$ for the concurrent runs of the La Jolla Nd standard. The $\varepsilon Nd(t)$ values were calculated using accepted parameters for CHUR (Bouvier *et al.* 2008). Model T_{DM} ages were calculated for a one-stage model; parameters for DM are after Goldstein & Jacobsen (1988). Results are presented in Table 8.

Sr isotopes and Rb and Sr concentrations were determined on an MI-1201-T mass spectrometer using Ta filaments. The measured Sr isotope compositions of the SRM-987 standard were normalized to the NBS recommended value of 0·71034. Errors of the measured Sr isotope compositions do not exceed 0·04% (2σ), and the errors for the Rb–Sr isotope ratios are below 1·5% (2σ). For calculation of initial isotope ratios, the decay constants of Steiger & Jäger (1977) were used. The Rb–Sr results are presented in Table 9.

The U–Pb composition of zircon and titanite from carbonatite was analyzed by isotope dilution thermal

Table 4: Representative carbonate compositions

Rock:	C1	C2		Ecl
Sample	TN-T4/07B	T-2-08		
Mineral:	Cc	Cc	Dol lam	Dol
FeO	2·21	1·68	5·55	5·94
MnO	0·17	0·11	0·16	0·07
MgO	3·26	2·23	17·23	17·07
CaO	48·17	48·05	28·74	29·87
SrO	0·73	0·55	0·32	—
Total	54·54	52·62	52·00	55·20
Fe	0·03	0·03	0·08	0·08
Mn	0·00	0·00	0·00	0·00
Mg	0·08	0·06	0·42	0·41
Ca	0·88	0·91	0·50	0·51
Sr	0·01	0·01	0·00	—
Total	1·00	1·00	1·00	1·00

Table 5: Representative bulk major and minor element compositions

Rock:	Carbonatite				Marble	Eclogite-kindred			Pyroxenite-kindred		
	C1			C2	M	E	CE	Gl-1	Grt-Px	Px	Gl-2
Sample:	T5/07	TS-10-1	TF-10-3	TN-2-08	TN-T1	TN-5-05	TS-5-11	T-16·3	TN-T6	TN-T8A	TN-T2-07
Lab.:	UiT	UiT	UiT	UiT	UiT	UiT	UiT	UiT	UiT	UiT	UiT
SiO_2	24·36	16·06	21·98	0·15	18·13	46·54	41·48	42·30	45·58	46·15	41·80
TiO_2	1·70	1·03	3·03	0·39	0·30	1·99	3·75	2·35	0·15	0·41	1·07
Al_2O_3	9·61	5·83	9·48	n.d.	5·26	14·68	10·98	11·85	12·96	9·51	8·54
Cr_2O3	n.d.	n.d.	n.d.	n.d.	n.d.	0·05	0·03	n.d.	n.d.	0·08	0·48
FeO	13·70	8·80	13·22	3·50	2·60	14·02	13·72	10·53	10·67	9·63	8·16
MnO	0·25	0·19	0·21	0·15	0·04	0·20	0·16	0·07	0·33	0·19	0·11
MgO	6·91	9·19	6·21	3·26	1·92	7·42	9·36	13·45	16·98	15·00	15·75
CaO	21·94	27·97	24·79	49·01	40·33	12·75	16·18	7·96	9·53	14·60	13·65
Na_2O	0·17	0·18	0·04	n.d.	0·34	2·26	1·56	1·26	0·66	0·87	0·75
K_2O	3·60	3·16	1·88	n.d.	0·96	0·07	0·02	5·60	0·38	1·87	4·51
P_2O_5	2·26	0·40	2·73	0·10	0·05	0·20	0·12	0·11	0·01	0·02	0·63
CO_2	15·54	24·29*	14·30*	37·34*	30·29	0·10*	2·19*	2·60*	0·23*	0·86*	3·06*
F*	0·17	0·10	0·17	0·01	0·02	0·03	0·01	0·16	0·01	0·06	0·18
O = –F	0·07	0·04	0·07	0·00	0·01	0·01	0·01	0·07	0·00	0·02	0·08
Total	100·14	97·15	97·97	93·76	100·24	100·29	99·54	98·17	97·49	99·22	98·61
Mg#	50·0	67·4	48·2	64·8	59·4	51·2	57·4	71·6	75·9	75·5	79·2

E, eclogite; CE, carbonated eclogite; Gl-1, glimmerite after eclogite; Gl-2, glimmerite after pyroxenite; n.d., not detected; n.a., not analyzed.
*Analyzed in Geological Institute KSC, Apatity.

Table 6: Representative whole-rock trace element compositions

Rock:	Carbonatite					Marble	Eclogite-kindred					Pyroxenite-kindred		
	C1				C2	M	E		CE	MS-E	Gl-1	Px	Px	Gl-2
Sample:	T5/07	TS-10-1	TF-10-3	TN-2-08		TN-T1	TN-5-05	TS-1-11	TS-5-11	TS-8-11	T-16.3	TN-T6	TN-T8A	TN-T2-07
Lab:	NGU	UiT	UiT	UiT		NGU	UiT	UiT	UiT	UiT	NGU	NGU	NGU	NGU
Rb	104	71	67	b.d.l.	43		5·4	3·3	5·5	44	194	16	63	165
Ba	3280	963	1057	79	140		33	3·7	8·6	359	1760	221	621	1740
Th	b.d.l.	1·3	2·7	4·1	8·2		b.d.l.	b.d.l.	b.d.l.	b.d.l.	1·0	0·9	0·2	1·0
U	b.d.l.	b.d.l.	b.d.l.	b.d.l.	3		b.d.l.	b.d.l.	b.d.l.	n.a.	0·30	0·35	b.d.l.	0·30
Nb	8·87	b.d.l.	11	3·0	6·33		8	7	30	20	3·30	0·57	0·90	3·05
Ta	0·45	n.a.	n.a.	n.a.	0·45		n.a.	n.a.	n.a.	n.a.	0·20	0·06	b.d.l.	0·20
La	223	104	72	226	23·6		11	b.d.l.	10	6	8·8	5·5	5·8	28·0
Ce	446	221	159	414	45·5		12	13	18	14	21·5	12·9	18·0	71·2
Pb	21·4	14	27	45	10·7		2·20	2·70	2·50	3·60	23·1	11·4	22·8	24·4
Pr	56	n.a.	n.a.	n.a.	5·11		n.a.	n.a.	n.a.	n.a.	2·50	1·56	2·45	9·60
Sr	2080	2767	1544	3764	1510		63	38	166	115	210	105	202	374
Nd	229	114	90	181	19·1		6·9	4·5	13	6·3	11·50	7·72	12·4	43·3
Hf	7·68	n.a.	n.a.	n.a.	1·66		n.a.	n.a.	n.a.	n.a.	1·55	0·67	1·00	4·65
Zr	370	32	45	51	66		100	88	67	39	46	35	40	206
Sm	38·4	23	16	46	3·62		3·7	3·8	5·3	2·9	2·55	2·33	3·00	9·60
Eu	8·58	n.a.	n.a.	n.a.	0·67		n.a.	n.a.	n.a.	n.a.	0·60	0·79	0·85	2·15
Gd	23·1	n.a.	n.a.	n.a.	2·6		n.a.	n.a.	n.a.	n.a.	1·75	3·1	2·25	5·60
Tb	2·83	n.a.	n.a.	n.a.	0·42		n.a.	n.a.	n.a.	n.a.	0·20	0·75	0·40	0·70
Dy	11·7	n.a.	n.a.	n.a.	2·38		n.a.	n.a.	n.a.	n.a.	1·00	5·87	2·90	2·65
Ho	1·83	n.a.	n.a.	n.a.	0·49		n.a.	n.a.	n.a.	n.a.	0·13	1·63	0·75	0·37
Y	48·8	26	22	12	12·7		38	34	29	19	4·15	43	19·9	10·1
Er	3·55	n.a.	n.a.	n.a.	1·28		n.a.	n.a.	n.a.	n.a.	0·30	5·32	2·45	0·70
Tm	0·45	n.a.	n.a.	n.a.	0·2		n.a.	n.a.	n.a.	n.a.	b.d.l.	0·97	0·40	b.d.l.
Yb	2·47	n.a.	n.a.	n.a.	1·33		n.a.	n.a.	n.a.	n.a.	b.d.l.	7·23	2·85	0·40
Lu	0·33	n.a.	n.a.	n.a.	0·2		n.a.	n.a.	n.a.	n.a.	b.d.l.	1·16	0·49	0·05
Sc	b.d.l.	21	17	39	b.d.l.		40	42	24	20	10	59	42	10
V	226	156	314	4	24		383	368	410	432	344	133	209	181
Cr	62	14	174	17	65		373	453	219	149	80·9	3880	539	2840
Co	19	16	19	2	b.d.l.		44	45	39	30	44	62	69	38
Ni	b.d.l.	3	4	8	b.d.l.		62	82	53	16	21	184	31	347
Cu	b.d.l.	16	14	11	9		37	58	81	9	14	75	46	25
Zn	284	80	278	47	40		113	107	106	134	120	31	48	142
Ga	11	7	11	b.d.l.	6		20	19	16	14	20	5	9	12

b.d.l., below detection limit; n.a., not analyzed.

Table 7: Stable C and O isotope compositions of carbonatite and marble

Sample	Rock type	$\delta^{13}C_{V\text{-}PDB}$	$\delta^{18}O_{V\text{-}SMOW}$
TN-2	Carbonatite	1·9	10·5
TN-3	Carbonatite	1·5	10·6
TN-8	Carbonatite	–1·4	11·0
TN-4B	Carbonatite	0·1	11·4
TN-T1	Marble	4·6	19·5
TN-4	Marble	0·2	17·9
TN-7	Marble	3·3	22·9

ionization mass spectrometry (ID-TIMS) at the University of Oslo. Details of the procedure have been described by Corfu (2004). The results of the U–Pb analyses are shown in Table 10.

In the following, the Mg-number (Mg#) of rocks and ferromagnesian minerals is defined as the molar proportion $100Mg/(Mg + Fe_{total})$.

PETROGRAPHY AND MINERAL COMPOSITIONS

Carbonatite

There are two types of the Tromsø carbonatite. The major type, in this study termed C1, is rich in silicate minerals. Biotite-rich varieties are most common (Fig. 3i), but varieties almost devoid of biotite also occur (Fig. 3j). Major primary matrix phases of the C1 carbonatite are Mg–Fe-calcite ± Fe-dolomite + garnet + clinopyroxene + Ti-rich Mg-biotite/phlogopite. Minor phases are allanite/REE (rare earth element)-clinozoisite, apatite, rutile, ilmenite, zircon, monazite and pyrite.

Type-C2 carbonatite occurs as veins and patches within type C1 (Fig. 3g and l). The primary magmatic assemblage is Mg–Fe-calcite (>90%) with minor clinopyroxene, garnet, phlogopite, allanite/REE-clinozoisite, apatite, rutile, zircon and monazite.

Broska *et al.* (2014) reported analyses of garnet, biotite, clinopyroxene, apatite and calcite from the carbonatite.

Clinopyroxene

Clinopyroxene has a faint green color in thin section, and apparently occurs in two modes. The first mode is megacrysts (up to 5 cm across) of Cr-diopside (Fig. 3k) with rods of phlogopite and amphibole, which are mainly oriented parallel to the *c*-axis. Bulk analysis (XRF) of a fragment of megacryst (sample TN-T4A; Fig. 3k) gives

Table 8: Sm–Nd concentrations and isotope compositions

Sample	Rock	Age (Ma)	Sm (ppm)	Nd (ppm)	Sm/Nd	147/144	143/144	Err	ε(0)	ε(*t*)	T(DM)	T(DM-2)	T(CHUR)	$I_{Nd}(t)$
NT-10.1	C1	450	22·583	84·989	0·26572	0·160633	0·512507	13	–2·56	–0·48	1848	1243	556	0·512034
T-4/07	C1	450	29·550	165·712	0·17832	0·107784	0·512296	16	–6·67	–1·56	1231	1332	588	0·511978
TN-T3	C1	450	15·688	81·704	0·192	0·116055	0·512361	16	–5·41	–0·77	1234	1266	525	0·512019
TF-10-16	C1	450	37·772	237·745	0·15887	0·096030	0·512240	18	–7·77	–1·98	1180	1367	604	0·511957
TF-10-4	C1	450	28·224	148·108	0·19056	0·115285	0·512290	19	–6·79	–2·11	1332	1377	652	0·511950
T-1A-08	C2	450	36·548	280·581	0·13026	0·078733	0·512120	15	–10·11	–3·33	1165	1479	671	0·511888
TS-5-11	CE	450	5·066	13·776	0·36771	0·222260	0·512486	10	–2·97	–4·44	–12218	1571	–909	0·511831
TS-8-11	ME	450	3·822	11·010	0·34714	0·209826	0·512681	15	0·84	0·08	17949	1196	495	0·512062
TS-2/11	E	450	4·220	12·651	0·33357	0·201624	0·512528	7	–2·15	–2·43	7756	1404	–3387	0·511934
TN-5/05	E	450	3·659	12·684	0·2885	0·174381	0·512402	6	–4·61	–3·33	2893	1478	1616	0·511888
TØ-103	M	450	0·358	1·535	0·23329	0·141010	0·512392	460	–4·80	–1·60	1591	1335	675	0·511976
NT-10.3	M	450	1·481	8·617	0·17187	0·103926	0·512279	16	–7·00	–1·67	1211	1341	591	0·511973

Table 9: Rb–Sr concentrations and isotope compositions

Sample	Rock	Rb (ppm)	Sr (ppm)	Rb/Sr	$^{87}Rb/^{86}Sr$	$^{87}Sr/^{86}Sr$	±Δ%	T (Ma)	ISr(*t*)	εSr(*t*)
NT-10.1	Carbonatite C1*	1·096	5089·9	0·000	0·000623	0·70689	7	450	0·706886	41·7
TF-10-16	Carbonatite C1*	5·75	2964·7	0·002	0·005472	0·70592	13	450	0·705885	27·5
T-4/07	Carbonatite C1*	46·86	1653·6	0·028	0·079953	0·70694	14	450	0·706427	35·2
TN-T3	Carbonatite C1*	49·75	1745·5	0·029	0·080415	0·70644	15	450	0·705925	28·0
TF-10-4	Carbonatite C1*	66·02	1577·4	0·042	0·118086	0·70727	14	450	0·706513	36·4
T1A/08	Carbonatite C2*	0·17	4180·1	0·000	0·000115	0·70688	15	450	0·706879	41·6
NT-10.3	Marble	5·28	506·6	0·010	0·030259	0·70813	8	450	0·707936	56·6
TO-103	Marble	0·4	1035·3	0·000	0·001090	0·70599	12	450	0·705983	28·9
TN-5/05	Eclogite	3·65	60·58	0·060	0·169992	0·70951	13	450	0·708420	63·5
TS-2/11	Eclogite	0·36	61·95	0·006	0·016396	0·70989	16	450	0·709785	82·9
TS-5-11	Carbonate-rich eclogite*	1·12	161·6	0·007	0·019554	0·70638	14	450	0·706255	32·7
TS-8/11	Metasomatized eclogite*	43·77	121·2	0·361	1·018916	0·71323	15	450	0·706698	39·0

*Samples used for errochron plot (Fig. 7c).

Table 10: U–Pb analyses of zircon and titanite from the Tønsvika carbonatite

Fraction	Weight (μg)	U (ppm)	Th/U*	Pb com†	$^{206}Pb/^{204}Pb$‡	$^{207}Pb/^{235}U$§	2σ (abs)	$^{206}Pb/^{238}U$§	2σ (abs)	rho
Z eq sbr [9]	10	55	0·52	1·3	1928	0·5766	0·00300	0·07375	0·00026	0·70
Z eq sbr [2]	7	29	0·38	2·0	481	0·5608	0·00820	0·07247	0·00027	0·44
Z sp sh [1]	8	1822	0·81	2·8	23 645	0·5558	0·00128	0·07190	0·00015	0·96
Z sp zh [12]	12	662	0·81	6·9	5124	0·5504	0·00139	0·07124	0·00015	0·90
Z lp sh [1]	1	2426	0·62	1·6	6902	0·5584	0·00166	0·07226	0·00019	0·89
Z lp sh [1]	1	928	0·51	1·1	3899	0·5515	0·00187	0·07131	0·00021	0·78
T y NA [2]	95	10	25·9	452	42·74	0·5459	0·0642	0·0726	0·0010	0·01
T y-b NA [4]	234	11	28·7	1257	42·26	0·5669	0·0661	0·0726	0·0011	0·02

Fraction	$^{207}Pb/^{206}Pb$	2σ (abs]	$^{206}Pb/^{238}U$ age (Ma)	2σ	$^{207}Pb/^{235}U$§ age (Ma)	2σ	$^{207}Pb/^{206}Pb$§ age (Ma)	2σ	Disc. (%)¶
Z eq sbr [9]	0·05670	0·00021	458·7	1·6	462·3	1·9	480·0	8·2	4·6
Z eq sbr [2]	0·05613	0·00075	451·0	1·6	451·1	5·3	457·5	29·4	1·5
Z sp sh [1]	0·05606	0·00004	447·6	0·9	448·8	0·8	454·8	1·5	1·6
Z sp zh [12]	0·05603	0·00006	443·6	0·9	445·2	0·9	453·6	2·4	2·3
Z lp sh [1]	0·05604	0·00008	449·8	1·1	450·5	1·1	454·1	3·0	1·0
Z lp sh [1]	0·05609	0·00012	444·0	1·3	446·0	1·2	456·1	4·8	2·7
T y NA [2]	0·0545	0·0065	451·7	6·4	442	41			
T y-b NA [4]	0·0567	0·0066	451·5	6·6	456	42			

Key for fraction analyzed: Z, zircon; T, titanite; eq, equant; sp, short prismatic; lp, long prismatic; sbr, subrounded; sh, subhedral; y, yellow; b, brown; NA, non-abraded (all zircons abraded); [*n*], number of grains.
*Model value calculated from $^{208}Pb/^{206}Pb$ ratio and the age of the sample.
†Total common lead, including analytical blank and initial common lead in the sample.
‡Corrected for spike contribution and fractionation.
§Corrected for spike contribution, fractionation, blank and initial common lead (as calculated from Stacey & Kramers, 1975); errors reported at 2σ.
¶Degree of discordance.

0·55 wt % K_2O and 0·24 wt % Cr_2O_3 with Mg# ~ 85, and the corresponding structural formula (based on 6 oxygen) is

$$K_{0·03}Na_{0·07}Ca_{079}Mg_{0·88}Fe^{2+}0·15Cr_{0·01}Ti_{0·01}Al^{tot}0·17Si_{1·93}O_6.$$

Microprobe spot analysis of the host clinopyroxene shows 0·32 wt % Cr_2O_3 and no detectable K_2O, giving the formula

$$Na_{0·10}Ca_{0·88}Mg_{0·78}Fe^{2+}0·14Cr_{0·01}Al^{tot}0·14Si_{1·98}.$$

The second mode is matrix clinopyroxene richer in Na, poor in Cr, and lower in Mg (70) (Fig. 4a). Exsolution features with rods of phlogopite oriented parallel to the *c*-axis and lamellae of Fe–Ti-oxides oriented approximately parallel to {001} are occasionally observed in larger matrix grains (Fig. 5c). Smaller grains in matrix and as inclusions in garnet do not show such features. Clinopyroxene occurs together with calcite, apatite, rutile and ilmenite in polyphase inclusions in garnet (Figs 5d and 6i). Clinopyroxene locally shows partial breakdown to vermicular intergrowth textures of hornblende and quartz, or is rimmed by hornblende.

Garnet

Garnet occurs as large (up to 10–15 mm) subhedral grains and is commonly poikilitic with numerous inclusions of all the other primary matrix phases (Fig. 6b, e and i). Both single-phase and polyphase inclusions are present (Figs 5d and 6i). Radial cracks around inclusions of calcite (Fig. 6c) and zircon are common (Fig. 6e). In some samples, garnet rims are partially corroded and replaced by late phlogopite and/or allanite/REE-epidote (Fig. 5h). The composition of garnet in terms of end members is $And_{5·4–6·6}Gr_{23–31}Sp_{1·9–2·4}Alm_{43–53}Py_{15–20}$ (Fig. 4b).

Phlogopite

Phlogopite (Table 3) appears in four modes: (1) pale brown flaky crystals with random orientation (Fig. 6a) in the matrix of type C1 (sample TN-T4/07B with Mg# = 55–57 and 3·6 wt % TiO_2), and type C2 with Mg# = 65–66 and 2·7–2·9 wt % TiO_2); (2) small inclusions in garnet; (3) rods (Mg# = 49–53, 4·2–4·3 wt % TiO_2; sample TN-T4/07B) oriented along the *c*-axis in clinopyroxene; (4) as a replacement of garnet. Close to the contact with eclogite and garnet pyroxenite, the amount of phlogopite in C1 is drastically reduced. In the Cr-diopside megacrysts of sample TN-T4A (Fig. 3k), the rods of phlogopite have a high Mg# (80·4) and a lower TiO_2 content (~1·7 wt %) compared with the matrix phlogopite in the same sample, which has Mg# = 69·4 and TiO_2 ~3·0 wt % (Table 3).

Mg–Fe-calcite and Fe-dolomite (Table 4)

Mg–Fe-calcite occurs as a major phase in the matrix and as abundant inclusions in garnet, clinopyroxene and other phases. Inclusions of Mg–Fe-calcite are typically subrounded and commonly surrounded by radial cracks (Fig. 6c). Exsolved lamellae of Fe-dolomite are common in matrix Mg–Fe-calcite, mostly in central parts of the grains, whereas rims are virtually lamellae-free (Fig. 5a). Matrix calcite hosts numerous minute inclusions of pyrite and monazite. In more Mg-rich rocks, Fe-dolomite with lamellae of calcite is observed (Fig. 5b). Broska *et al.* (2014) presented compositions of calcite from two C1 samples. In both samples, the composition is $Ca_{0·88–0·89}Mg_{0·06}Fe_{0·03}(CO_3)$, with ~0·7 wt % SrO (Broska *et al.*, 2014, table 3). Broska *et al.* (2014) also presented compositions of Ca–Dol perthite with the composition $Ca_{0·77–0·79}Mg_{0·12–0·13}Fe_{0·05}(CO_3)$ with ~0·5 wt % SrO. In C2 sample T-2-08 Mg–Fe calcite has the composition $Ca_{0·91}Mg_{0·06}Fe_{0·03}(CO_3)$, whereas exsolved lamellae of Fe-dolomite are $Ca_{0·50}Fe_{0·08}Mg_{0·42}(CO_3)$ with ~0·30 wt % SrO.

Apatite

Apatite is present in amounts varying from <1 to 10 modal % of the rock. It occurs in three modes: (1) as randomly oriented, elongated sub- to euhedral crystals in the matrix (Fig. 6a and h); (2) as larger sub- to euhedral inclusions in garnet and clinopyroxene (Fig. 6b); (3) as tiny (15 μm × 50 μm) euhedral crystals included in garnet (Figs 5d and 6i). Larger apatite grains in the matrix commonly contain rods of quartz and $Fe_{1-x}S$ (pyrrhotite), which are oriented along the *c*-axis of the host apatite (Broska *et al.*, 2014). Locally, lamellae of Fe-dolomite in

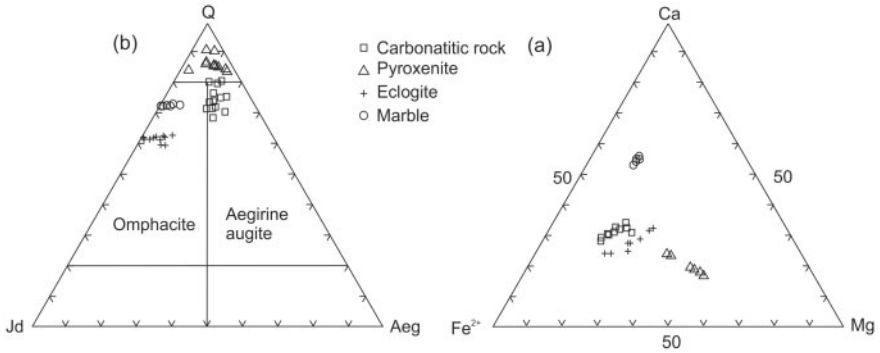

Fig. 4. Compositional variations of (a) garnet and (b) clinopyroxene in carbonatite, pyroxenite, eclogite and marble.

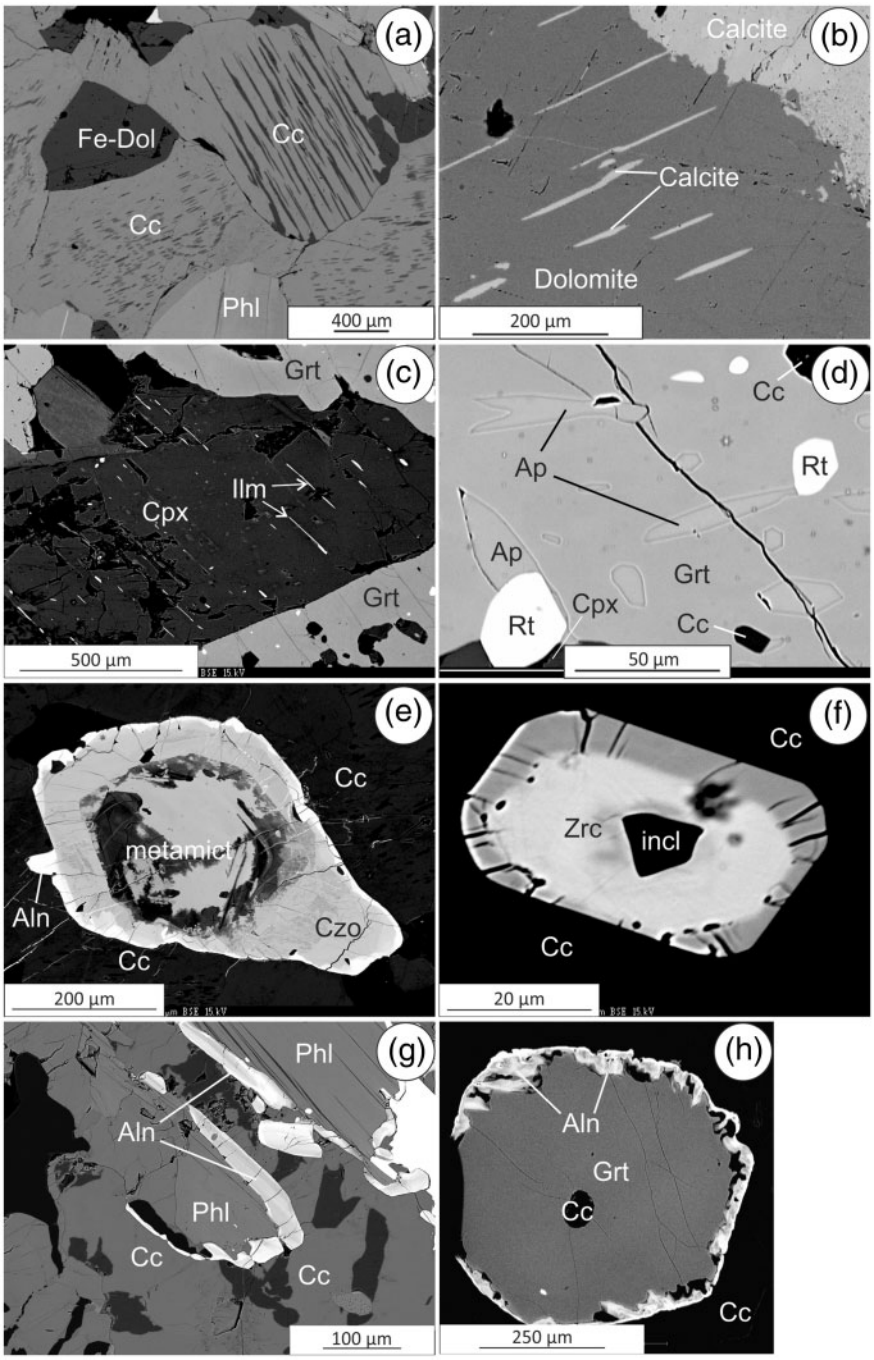

Fig. 5. Electron backscatter images. (a) Calcite with exsolved lamellae of Fe-dolomite in C1 carbonatite. (b) Lamellae of calcite in dolomite next to altered calcite grain (C1). (c) Clinopyroxene in C1 carbonatite, showing exsolution lamellae of ilmenite oriented along (001). This pyroxene also has rods of phlogopite oriented along the *c*-axis. (d) Inclusions of sub- to euhedral apatite and polyphase inclusions of apatite + rutile + clinopyroxene in garnet (C2). (e) Strongly zoned clinozoisite–allanite in C2 carbonatite. The inner part is metamict, and the bright rim is enriched in REE. (f) Zoned euhedral zircon in C2 carbonatite, with U-enriched core in calcite matrix. The inclusion consists of at least three phases that are too small for identification. The radial fracturing of the low-U rim of the grain should be noted. (g) Late allanite growing along interfaces of phlogopite and matrix calcite, C1 carbonatite. (h) Garnet, partially replaced by allanite, in calcite matrix of C2 carbonatite.

apatite are also observed (Broska *et al.*, 2014). Apatite grains without exsolution textures, occurring in garnet, show blue cathodoluminiscence, whereas those in the matrix have green luminescence (Fig. 6n). The small euhedral inclusions of apatite within garnet have a higher content of Fe than those occurring in the matrix (>0·88 vs <0·20 wt % FeO). Apatite is relatively F-rich ($X_F = 0·45$–0·65; Broska *et al.*, 2014), and some grains are spatially associated with monazite (Fig. 6h), although no signs of exsolution of monazite from apatite have been observed.

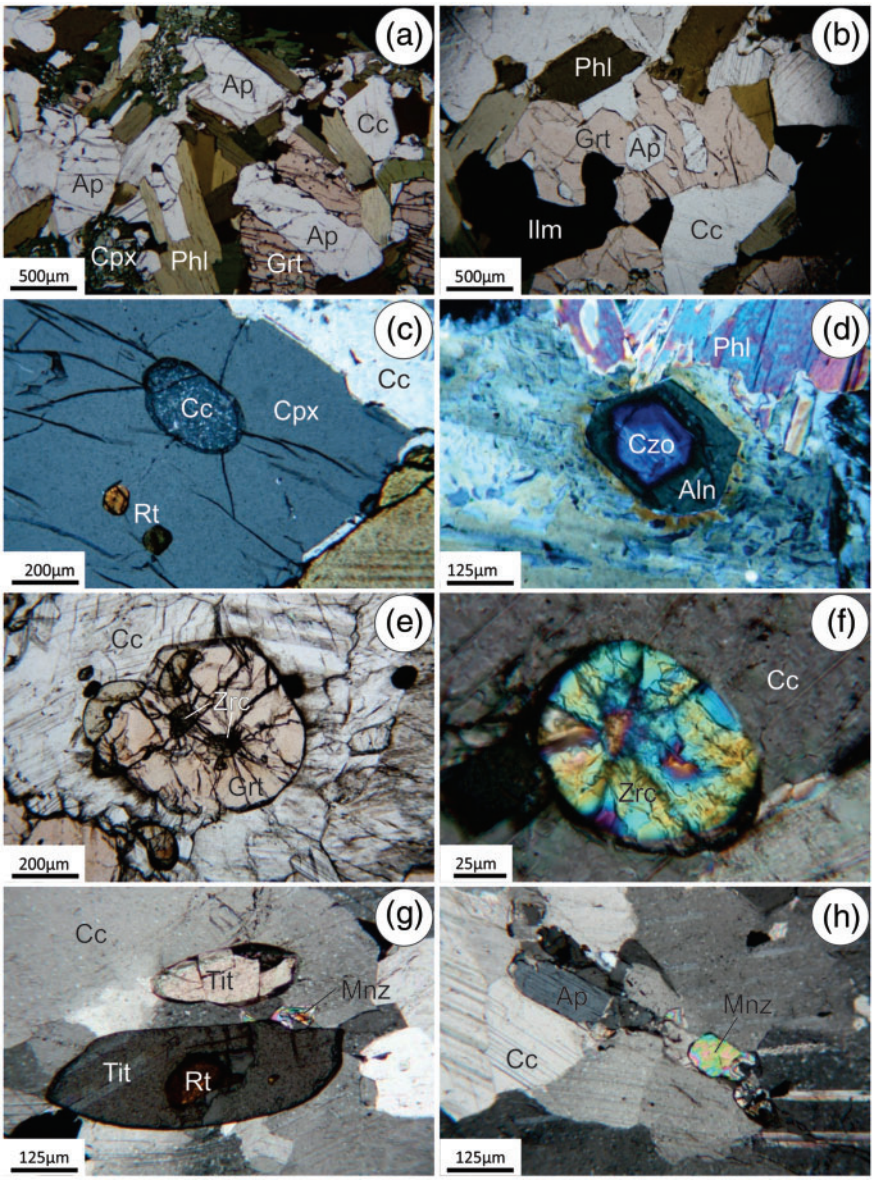

Fig. 6. Photomicrographs of various rock-types and microtextures. (a) C1 carbonatite with Grt–Cpx–Cc–Phl–Ap. (b) C2 carbonatite with Grt–Cc–Phl–Ap–Ilm. (c) Inclusion of calcite in clinopyroxene. Radial fractures should be noted. (d) Zoned euhedral clinozoisite–allanite with pleochroic halo in phlogopite-rich C1 carbonatite. (e) Garnet with inclusions of zircon in C2 carbonatite. The radial fractures emanating from zircon should be noted. (f) Radially fractured rounded zircon in C2 carbonatite. (g) Rutile overgrown by titanite in C1 carbonatite. (h) Separate grains of apatite and monazite in C2 carbonatite. (i) Numerous small inclusions of calcite, apatite, clinopyroxene, rutile and ilmenite in large garnet grain; C1 carbonatite. (j) Oriented rods of phlogopite and hornblende in Cr-diopside from pyroxenite. It should be noted that the rim of diopside against matrix phlogopite is devoid of these rods. (k) Oriented rods of phlogopite in Cr-diopside in pyroxenite viewed oblique to {001}. (l) Needles of rutile oriented in two directions in diopside (metasomatized eclogite). (m) Needles of rutile oriented in three directions in large garnet (Cr-poor pyroxenite). (n) CL image of an apatite-rich C1 carbonatite (apatite included in garnet shows blue luminescence, and apatite in matrix is green).

Allanite/REE-clinozoisite

Allanite/REE-clinozoisite occurs in two modes. Euhedral and strongly zoned crystals are present in a few samples (Figs 5e and 6d). The central Th-rich part (Th ~2 wt %) of these grains is metamict and surrounded by a crystalline rim showing enrichment in REE and oscillatory zoning. A pleochroic halo is commonly present in minerals in contact with this allanite/REE-clinozoisite (Fig. 6d). Low-Th allanite commonly occurs as rims between matrix calcite and silicates, mainly phlogopite (Fig. 5g), but is also seen to replace garnet rims (Fig. 5h). This late allanite is also strongly zoned with respect to REE content. Total REE content reaches ~25 wt % (work in progress).

Fe–Ti-oxides. Fe–Ti-oxides are present as ilmenite and rutile. Both minerals are abundant, and are also in mutual contact. They form inclusions in garnet and occur also in the matrix. Separate grains of ilmenite always show exsolution lamellae of hematite or magnetite

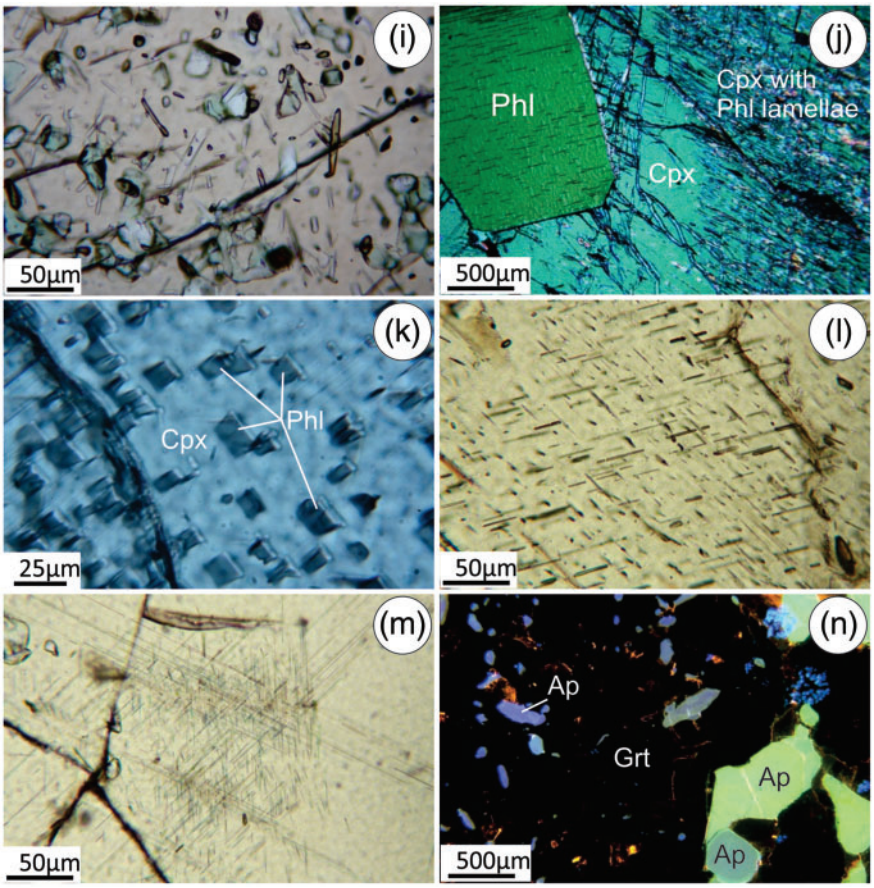

Fig. 6. Continued.

(Broska *et al.*, 2014, fig. 3G). Ilmenite is also present as lamellae in large grains of clinopyroxene (Fig. 5c). Within the matrix, titanite (Fig. 6g) commonly overgrows rutile.

Zircon

Zircon, either as sub- to euhedral or rounded grains, occurs as inclusions in garnet (Fig. 6e) and other major phases or as a matrix phase (Fig. 6f). The sub- to euhedral grains show oscillatory zoning with U-rich cores and U-poor rims (Fig. 5f). The outer zone is commonly fractured, with radial cracks emanating from the apices of the central U-rich parts. When included in garnet, the host garnet also shows radial cracks (Fig. 6e). The rounded grains appear homogeneous.

Monazite

Monazite occurs in three modes: (1) as larger, zoned, sub- to euhedral grains in the matrix (Fig. 6h); (2) as small, homogeneous, irregular grains commonly associated with apatite, titanite (Fig. 6g) or ilmenite; (3) as tiny grains within the matrix calcite.

Eclogite and metasomatized eclogite

The fairly massive and fine-grained (~1 mm) eclogite associated with carbonatite is essentially bimineralic (Ravna & Roux, 2006), with *c.* 60 modal % omphacite ($Jd_{11–36}Aeg_{1–10}Cats_{3–9}Quad_{57–69}$; Ravna & Roux, 2006; this paper), 35 modal % garnet ($Gr_{24–33}Alm_{37–48}Sp_{1–2}Py_{21–29}$; Ravna & Roux, 2006; this study) and minor phengite (3·39 Si atoms per formula unit; Ravna & Roux, 2006), rutile, quartz, and secondary diopside, hornblende, plagioclase, biotite and titanite. Locally, the eclogite shows a texture with alternating seams or laminae enriched in omphacite and garnet, respectively (Fig. 3a and b). This eclogite variety is commonly specked throughout with ~5% of calcite. In direct contact with carbonatite, the eclogite is coarse-grained and strongly enriched in phlogopite and carbonate minerals (Fig. 3a and b). In this metasomatized coarse-grained eclogite, diopside grains (Mg# = 89) are up to 20–30 mm across, often showing exsolution of rutile in two crystallographic directions (Fig. 6l). Coarse garnet grains (Mg# = 60) also contain needles of rutile, commonly oriented in three directions at ~120° (Fig. 6m). Dark brown biotite replacing garnet also shows this sagenitic texture. Dolomite occurs in some eclogite samples, with a composition of $Ca_{1·02}Mg_{0·82}Fe_{0·16}(CO_3)_2$.

Garnet–phlogopite-clinopyroxenite

This rock is relatively coarse-grained (3–30 mm; Fig. 3m), consisting of 60–90% deep green Cr-diopside

($Cr_2O_3 = 0{\cdot}2$–$0{\cdot}30$ wt %; Mg# = 86–89), 5–30 modal % Mg-rich garnet ($Gr_{31–38}Sp_{0{\cdot}9–1{\cdot}5}Alm_{31–38}Py_{37–50}$) containing up to 0·29 wt % Cr_2O_3, and with minor rutile, phlogopite ± dolomite ± apatite. Close to the contact with carbonatite the amount of phlogopite increases to >50 modal % of the rock, which then qualifies as a glimmerite (Fig. 3n). The central parts of Cr-diopside contain a high density of phlogopite rods (Fig. 6j and k), but the rims are almost devoid of lamellae (Fig. 6j). Most of these rods are oriented parallel to the cleavage planes of the host diopside. Bulk analysis (XRF) of a fragment of a large diopside gave 0·31 wt % K_2O and 0·38 wt % Cr_2O_3, with the corresponding structural formula (based on six oxygen)

$$K_{0{\cdot}01}Na_{0{\cdot}06}Ca_{0{\cdot}83}Mg_{0{\cdot}96}Fe^{2+}0{\cdot}11Cr_{0{\cdot}01}Al^{tot}0{\cdot}06Si_{1{\cdot}97}O_6.$$

An EDS scan analysis across one of the Cr-diopside grains gave similar results:

$$K_{0{\cdot}01}Na_{0{\cdot}08}Ca_{0{\cdot}84}Mg_{0{\cdot}91}Fe^{2+}0{\cdot}10Cr_{0{\cdot}01}Al^{tot}0{\cdot}09Si_{1{\cdot}98}O_6.$$

Marble and calc-silicate marble

The fine- to medium-grained, light grey country-rock marble is banded and foliated, and consists essentially of Fe- and Mg-poor calcite with variable contents of grossular-rich garnet, omphacite and zoisite, and accessory quartz and titanite. Calcite shows no sign of exsolution, and has a uniform composition. Garnet is fairly homogeneous and strongly enriched in grossular and depleted in the pyrope components ($Gr_{55{\cdot}9}Sp_{0{\cdot}7}Alm_{30{\cdot}2}Py_{13{\cdot}2}$) compared with the garnet in the carbonatite. Clinopyroxene is relatively rich in Na ($X_{Na} = 0{\cdot}24$) compared with that occurring in carbonatite, and zoisite has negligible contents of REE.

AGE CONSTRAINTS

U–Pb age

Two populations of zircon were separated from segregations of Si-poor carbonatite: (1) prismatic zircon showing strong oscillatory zoning with a U-rich core and a U-poor, fractured rim; (2) equant subrounded grains, which are low in U. Titanite occurs as yellow to brown grains, locally with inclusions of rutile (Fig. 7a).

Four analyses of subhedral prismatic zircon define a discordia line with an upper intercept age of 454·5 ± 1·1 Ma (MSWD = 0·39), whereas one fraction of equant, subrounded, low-U zircon gives a slightly younger concordia age of 451·6 ± 1·7 Ma (MSWD = 0·19; Fig. 7b). Titanite ages overlap the two zircon ages within error (Table 10), but are imprecise owing to the 5 ppm initial Pb for only *c.* 10 ppm U. A notable feature is the very high Th/U (>25) of titanite versus more normal values in zircon (0·5–0·8). These ages overlap those of Corfu *et al.* (2003).

Rb–Sr errorchron

Rb–Sr isotope whole-rock data on carbonatite, carbonate-rich eclogite and metasomatized eclogite yield an errorchron of 469 ± 77 Ma (MSWD = 8·4), with an initial $^{87}Sr/^{86}Sr = 0{\cdot}70639$ (Fig. 7c).

BULK-ROCK COMPOSITIONS

Major elements

Major element concentrations in 52 rock samples (25 C1 and two C2 carbonatites, 10 eclogite samples, including carbonated and metasomatized varieties, five garnet pyroxenites, four glimmerites and six marbles or calc-silicate marbles) have been analyzed. Representative analyses are given in Table 5, and all analyses are available in the Supplementary Data Table S1.

Carbonatite

Seven of the 13 analyzed carbonatite samples contain >20 wt % SiO_2 (22–26·3 wt %), and should be classified as calcium silicocarbonatites (Le Maitre, 2002). Six of the analyzed samples contain SiO_2 in the range 12–19·8 wt %, and could be termed silicate-rich calcium carbonatite (Chakhmouradian *et al.*, 2008). In this paper these two groups are, for simplicity, combined and referred to as C1. Two samples of SiO_2-poor calcium carbonatite are referred to as C2.

Type C1 carbonatite has SiO_2 contents in the range of 12–27 wt %, $Al_2O_3 = 5{\cdot}5$–11 wt %, MgO = 5·6–9·2 wt % and CaO = 21–33·8 wt %. Relatively large variations in $TiO_2 = 1{\cdot}0$–$4{\cdot}3$ wt %, $K_2O = 0{\cdot}06$–$3{\cdot}6$ wt %, and $P_2O_5 = 0{\cdot}01$–$2{\cdot}84$ wt % reflect variable and, in some cases, relatively high modal contents of rutile, ilmenite, phlogopite and apatite. The content of Na_2O varies from below detection limit to 0·62 wt %, and MnO is also low (0·12–0·33 wt %). Mg# ranges from 40 to 67.

Type C2 carbonatite dikes and patches of silicate-poor carbonatite are virtually SiO_2- and Al_2O_3-free, have very high contents of CaO (~50 wt %), and moderate MgO and Fe_2O_3 (3·3–3·6 wt % and 3·4–3·5 wt %, respectively; Mg# is in the range 65–68), reflecting the composition of the dominant Fe–Mg-calcite. Other elements are present in amounts of less than 0·5 wt %.

Marble and calc-silicate marble vary in composition, dependent on the amount of silicates present. Whereas the contents of CaO (38–50·9 wt %) and SiO_2 (2·58–20·2 wt %) are within the same range as in the carbonatite, Al_2O_3 (<6·1 wt %), MgO (1·59–4·02 wt %), K_2O (<1·23 wt %) and Fe_2O_3 (0·26–2·94 wt %) are generally lower than in C1 carbonatite. Mg# is in the range of 56–97.

Eclogite

Eclogite has a basaltic composition, showing little variation in major elements, and has Mg# ~50, with a silica content in the range of 45·57–47·35 wt %, and CaO content from 11·7 to 12·75 wt %. Carbonate-rich eclogite has lower SiO_2 (39·44–42·97 wt %) and similar or higher CaO (12·08–16·18 wt %). The content of K_2O is low in apparently unaltered samples (0·01–0·02 wt %), but becomes more elevated with increasing degree of metasomatism. The TiO_2 content is generally higher in

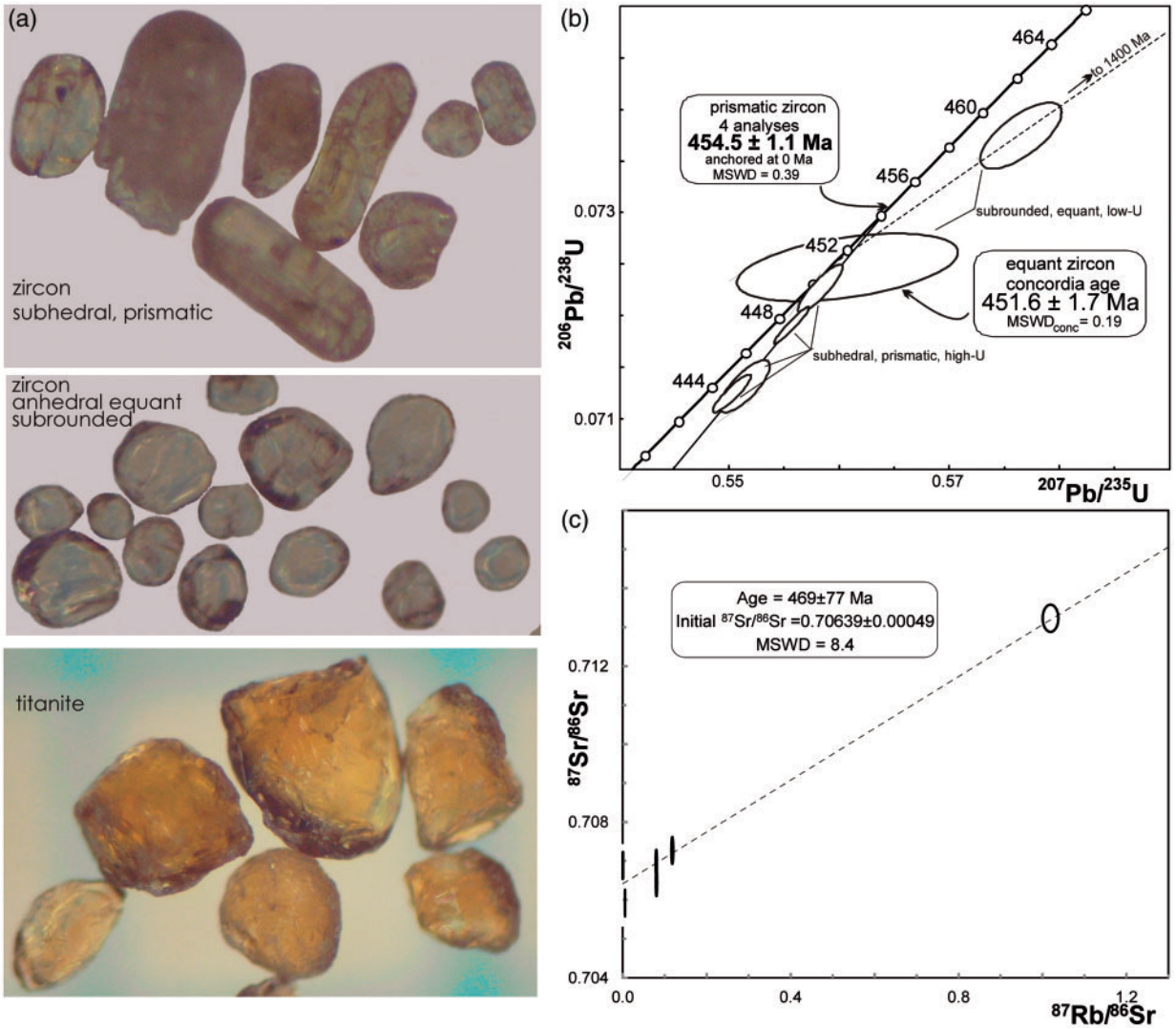

Fig. 7. (a) Separates of zircon and titanite used for age dating. (b) Concordia diagram showing the results of the U–Pb zircon dating. (c) Rb–Sr errorchron for carbonatites and carbonated and metasomatized eclogite from Tromsø Nappe.

the carbonate-rich and metasomatized samples than in the fresh ones.

Garnet pyroxenite

Garnet pyroxenite has major oxides in the following ranges: $SiO_2 = 45{\cdot}5$–50 wt %; $Al_2O_3 = 5$–13 wt %; $Fe_2O_3 = 4{\cdot}85$–$10{\cdot}7$ wt %; MgO = 14·8–17 wt % and CaO = 9·5–17 wt %. Mg# varies in the range 73·5–86. Minor oxide ranges are $TiO_2 = 0{\cdot}15$–$0{\cdot}40$ wt %, MnO = 0·10–0·33 wt %, $Na_2O = 0{\cdot}66$–$1{\cdot}07$ wt % and $K_2O = 0{\cdot}38$–$1{\cdot}87$ wt %. Potassium, hosted in phlogopite, correlates positively with TiO_2, indicating that titanium is mainly hosted in this mineral.

Glimmerite

Glimmerite occurs as two varieties, with the following characteristics. Samples T1/07, T2/07 and T3/07 have Mg# in the range 77·5–88·5. TiO_2 varies from 0·67 to 1·08 wt %. K_2O is in the range 4·51–6·99 wt %. Sample T-16.3 has Mg# = 69·5, $TiO_2 = 2{\cdot}35$ wt % and $K_2O = 5{\cdot}60$ wt %.

Based on the compositional characteristics, we infer that one type of glimmerite (high-Mg#) formed from phlogopitization of garnet pyroxenite and the other from alteration of eclogite. The variable and inverse correlation of CaO with K_2O indicates mutual replacement of these two components.

Trace elements

Trace element analyses of representative samples are given in Table 6, and all analyses are available in the Supplementary Data Table S1.

Type C1 carbonatite

Type C1 carbonatite is strongly enriched in large ion lithophile elements (LILE), particularly light REE (LREE), Sr (1300–2900 ppm) and Ba (150–3860 ppm) (Fig. 8a), compared with the primitive mantle (Palme & O'Neill, 2004). Mantle-normalized patterns show strong to moderate negative anomalies of Th, U, Nb, Ta, P, Zr, Hf and Ti (Fig. 8b). Vanadium (250–385 ppm)

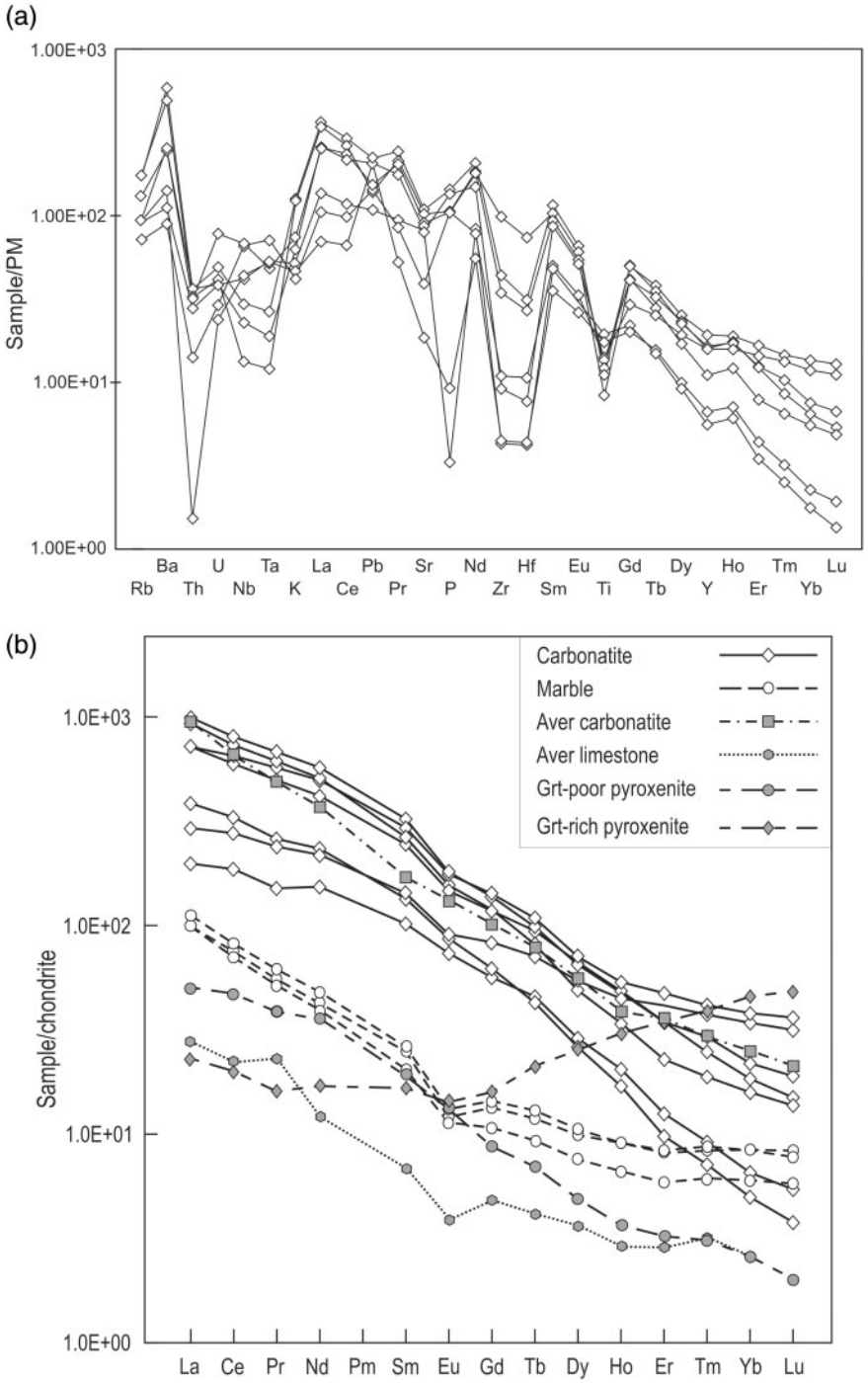

Fig. 8. (a) Primitive mantle (PM) normalized trace element patterns of carbonatite-like rocks and marble and (b) chondrite-normalized REE patterns. Curves for average carbonatite (Le Bas, 1999) and average limestone (Locke & Butler, 1993) are shown for reference. Chondrite and PM compositions used are taken from Palme & O'Neill (2004).

and Cr (46–275 ppm) are relatively high, whereas Ni and Co are at lower levels (16–24 and 10–27 ppm, respectively). Chondrite-normalized REE patterns (Fig. 8b) show negative slopes [$(La/Yb)_{n\text{-}chon} = 37–103$], which are similar to those for 'average' carbonatites (Le Bas, 1999), and only slightly negative Eu anomalies ($Eu/Eu^* = 0{\cdot}85–0{\cdot}97$).

Type C2 (dikes and patches of silicate-poor carbonatite)

Type C2 (dikes and patches of silicate-poor carbonatite) has high concentrations of Sr (3650–3760 ppm), La (200–225 ppm) and Ce (360–415 ppm), but moderate to low contents of other trace elements. Only XRF data are available for these rocks.

Marble and calc-silicate marble

Marble and calc-silicate marble also show negative REE slopes in mantle-normalized patterns (Fig. 8b), but not as steep as those for type C1 carbonatite $(La/Yb)_{n\text{-}chon} = 12{\cdot}1–16{\cdot}9$). The marbles have higher REE contents, but show the same overall pattern as 'average limestones' (Locke & Butler, 1993). Eu/Eu* ratios are significantly lower than for the carbonatite (0·67–0·77). The content of Sr (930–2330 ppm) in the Si-poor marble is significantly lower than that in the C2 carbonatite.

Eclogite

Eclogite has low contents of LILE. There is generally a significant increase of Rb and Ba in the carbonate-rich and metasomatically altered samples compared with the fresh ones. The contents of transition elements are similar to those of basaltic compositions, with Sc = 40–43 ppm, V = 368–386 ppm, Cr = 377–386 ppm, Co = 44–49 ppm, Ni = 48–82 ppm, Cu = 37–58 ppm, and Zn = 107–115 ppm. Carbonated eclogite has Sc = 23–27 ppm, V = 373–440 ppm, Cr = 176–502 ppm, Co = 29–54 ppm, Ni = 24–72 ppm, Cu = 22–104 ppm, and Zn = 100–120 ppm. Two samples of weakly metasomatized eclogite have the following contents of transition elements: Sc = 20–23 ppm, V = 420–432 ppm, Cr = 149–165 ppm, Co = 28–30 ppm, Ni = 16–21 ppm, Cu = 9–21 ppm and Zn = 117–134 ppm.

Garnet pyroxenite

Garnet pyroxenite is enriched in Cr (460–3880 ppm) and has moderate contents of V (130–210 ppm) and Ni (17–185 ppm). One garnet-rich sample shows a V-shaped chondrite-normalized REE pattern with slight enrichment of LREE as well as heavy REE (HREE) and a trough at intermediate REE (Fig. 8b). A garnet-poor sample (TN-T5) has a negative slope throughout and virtually no Eu anomaly (Eu/Eu* = 0·90–1·00).

Glimmerite

High-Mg# (77–89) glimmerite has high contents of Cr (2000–3180 ppm) and Ni (347–907 ppm). Other transition elements are V (130–180 ppm), Co (38–52 ppm), Cu (25–202 ppm), and Zn (41–142 ppm). Another variety with Mg# = 70 has 81 ppm Cr, 21 ppm Ni, and 360 ppm V. Both varieties are relatively rich in Rb (high Mg#: 165–330 ppm; low Mg#: 194 ppm) and Ba (high Mg#: 848–1740 ppm; low Mg#: 1760 ppm).

Stable isotopes

The C and O isotope ratios of bulk carbonate minerals are given in Table 7 and Fig. 9. The $\delta^{13}C_{(PDB)}$ values for the carbonatite range from –1·4 to 1·9, and $\delta^{18}O_{(SMOW)}$ from 10·5 to 11·0. The corresponding values for marble are 0·2–4·6 and 17·9–22·9, respectively (Table 7, Fig. 9). The $\delta^{18}O$ values of the carbonatite are distinctly lower than those of Paleozoic limestones (Fig. 9), represented by the marble or calc-silicate marble.

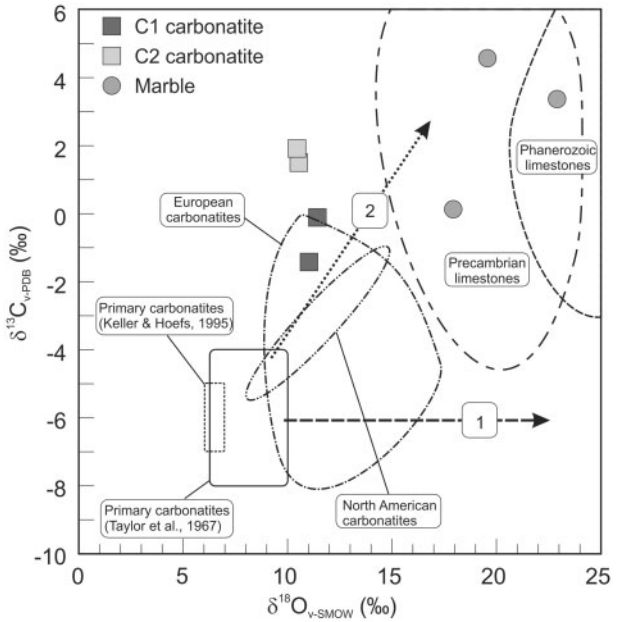

Fig. 9. Stable carbon and oxygen isotope compositions of Tromsø carbonatites and marbles. Boxes show isotope compositions of primary carbonatites (Taylor *et al.*, 1967, Keller & Hoefs, 1995). Fields for Precambrian and Phanerozoic limestones, and European and North American carbonatites after Bell (2005). Arrows indicate hydrothermal alteration (1) and high-*T* fractionation or sedimentary contamination (2) responsible for changes in isotopic compositions (Deines, 1989).

Strontium and neodymium isotopes

The radiogenic isotope signatures of Sr and Nd, with initial values for $^{87}Sr/^{86}Sr$ and $\varepsilon Nd(t)$ at $t = 450$ Ma, are presented in Table 8 and Fig. 10. Type C1 carbonatite has initial Sr-isotope ratios in the range 0·70589–0·70689, and $\varepsilon Nd(t)$ between –0·48 and –2·11. A sample of type C2 carbonatite has $(^{87}Sr/^{86}Sr)_i = 0{\cdot}70688$ and $\varepsilon Nd(t) = -3{\cdot}33$. Eclogite has initial Sr-isotope values in the range 0·70842–0·70979 and $\varepsilon Nd(t) = -2{\cdot}43$ to –3·33. A sample of carbonate-rich eclogite has a $(^{87}Sr/^{86}Sr)_i$ value of 0·70626 and $\varepsilon Nd(t)$ of –4·44. A metasomatized eclogite sample has $(^{87}Sr/^{86}Sr)_i = 0{\cdot}70670$ and $\varepsilon Nd(t) = +0{\cdot}08$. Initial values for marble are $(^{87}Sr/^{86}Sr)_i = 0{\cdot}70598–0{\cdot}70794$ and $\varepsilon Nd(t) = -1{\cdot}60$ to –1·67.

PRESSURE–TEMPERATURE CONDITIONS OF THE STUDIED ROCKS

Previous estimates

The UHP conditions for the Tromsø Nappe ($T \geq 750$°C and $P \geq 3{\cdot}5$ GPa) are constrained by the work of Ravna & Roux (2006) and Janák *et al.* (2012, 2013) and confirmed by the presence of microdiamonds (Janák *et al.*, 2013). Broska *et al.* (2014) obtained temperatures of 700–785°C using reintegrated compositions of calcite with dolomite exsolution lamellae from the carbonatite. These *P*–*T* conditions should be regarded as minimum values.

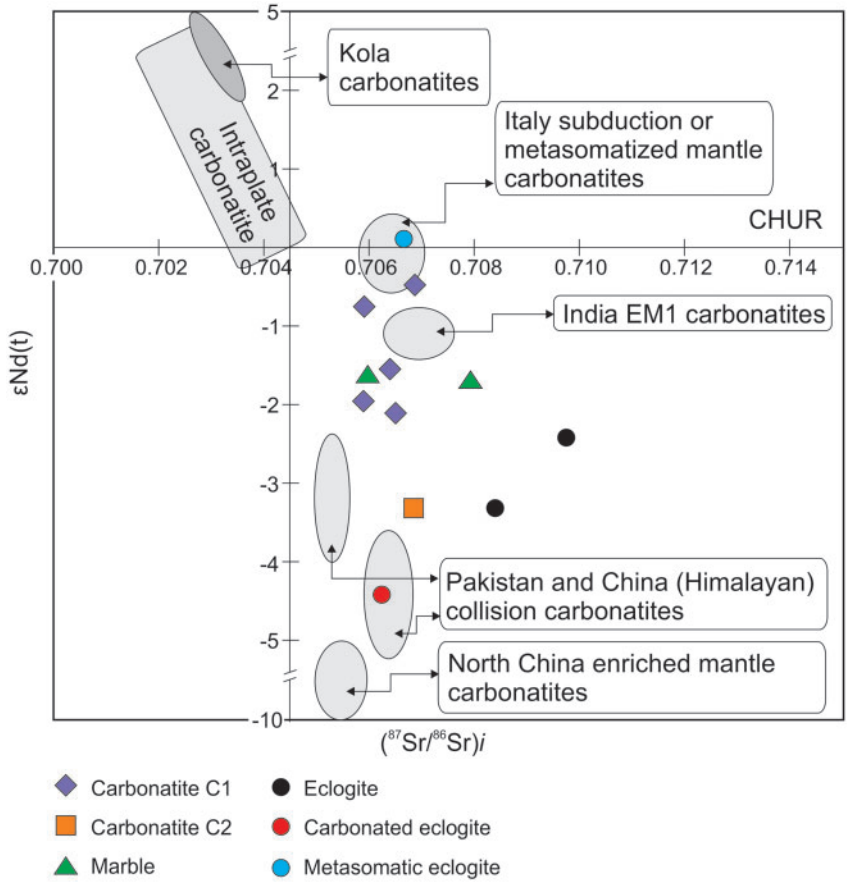

Fig. 10. εNd(*t*) vs $(^{87}Sr/^{86}Sr)_i$ for Tromsø carbonatite, marble and eclogite compared with intraplate, collision and subduction-related carbonatites worldwide. Data sources: intraplate carbonatites and Kola carbonatites, Rukhlov *et al.* (2015) and references therein; Italy, D'Orazio *et al.* (2007) and Rosatelli *et al.* (2007); India, Simonetti *et al.* (1995); Pakistan, Tilton *et al.* (1998); China (Himalayan), Hou *et al.* (2006); North China, Xu *et al.* (2011). Not shown but discussed in the paper are carbonatites from northeastern China (Ying *et al.*, 2004) with extremely radiogenic $^{87}Sr/^{86}Sr$ (0·7095–0·7106) and unradiogenic $^{143}Nd/^{144}Nd$ (–18·2 to –14·3).

Exsolution textures as indicators of high-*T*, high-*P* conditions

Petrographic observations of carbonatites and some of the associated rocks studied in this paper have revealed a variety of crystallographically oriented mineral inclusions in various minerals. These exsolution phenomena suggest original crystallization of the minerals at high-temperature and -pressure conditions.

Lamellar exsolution in carbonate

Lamellae of Fe-dolomite in calcite are ubiquitous in the carbonatite (Fig. 5a). These textures are classical examples of exsolution, where calcite can accommodate more Mg and Fe^{2+} in the structure at high *T*, but during cooling excess $Mg + Fe^{2+}$ will be expelled as dolomite (e.g. Anovitz & Essene, 1987). The accommodation of Fe^{2+} and Mg will also tend to stabilize calcite relative to aragonite to higher *P* (e.g. Kiseeva *et al.*, 2012). It is noteworthy that the dolomite lamellae in calcite mainly occur in the central parts of the grains, and that exsolved dolomite from the calcite rims apparently has migrated into the interstices or triple junctions between calcite grains (Fig. 5a), probably owing to recrystallization by strain-induced grain-boundary migration. In some samples, lamellae of calcite in Fe-dolomite are observed (Fig. 5b). According to Chakhmouradian *et al.* (2016), no convincing examples of this texture have previously been observed in carbonatites. Exsolution textures in carbonates in the spatially associated marbles have not been observed.

Lamellar exsolution in Fe–Ti oxides

The observation of ilmenite with lamellae of almost pure hematite or magnetite both as inclusions in garnet and as a matrix phase in the carbonatite (see Broska *et al.*, 2014, fig. 3G), is another line of evidence supporting a magmatic origin of the carbonatite. The ilmenite–hematite series is characterized by a miscibility gap (Lindsley, 1973). During slow cooling, the $FeTiO_3$–Fe_2O_3 solid solution tends to exsolve readily to yield lamellar intergrowths of ilmenite and hematite. If the conditions are reducing, hematite may be reduced to magnetite, but a distinction between these two minerals has not been addressed in this paper. No Fe–Ti-oxides have been observed in any of the other rock types in the area.

Rods of phlogopite in clinopyroxene

The occurrence of rods of phlogopite within clinopyroxene in the carbonatite and the associated clinopyroxenite or glimmerite (Fig. 6j and k) calls for an examination of possible mechanisms of these features. These rods are mainly oriented parallel to the *c*-axis in clinopyroxene. They are most common in the central parts of large clinopyroxenes, and virtually absent in the rims (Fig. 6j). Similar textures have been described earlier in garnet peridotite from SuLu, China, by Bozhilov *et al.* (2009) and in diamond-bearing marble from the Kokchetav Massif in Kazakhstan by Katayama *et al.* (2002) and Dobrzhinetskaya *et al.* (2009). Katayama *et al.* (2002) and Bindi *et al.* (2003) have described ultrapotassic clinopyroxene from the UHP rocks of the Kokchetav Complex. Experimental data have shown that high *P* increases the solubility of H_2O and K_2O in pyroxene (e.g. Harlow, 1997; Luth, 1997; Zhang *et al.*, 1997; Ogasawara *et al.*, 2002; Bromiley *et al.*, 2004). Hwang *et al.* (2004) argued that some of the well-aligned K-bearing inclusion pockets or lamellae in clinopyroxene from UHP rocks of the Kokchetav Massif could also have formed from intruding K-rich melts through partings or cleavages of the host pyroxene.

In the present case, the high density of such aligned rods in the central parts and their prominent absence in the rims of clinopyroxene (Fig. 6j) appear to be analogous to the dolomite exsolutions in calcite. Therefore, an exsolution process during uplift and cooling from an originally K_2O–H_2O-bearing clinopyroxene is favored here.

Ilmenite lamellae in clinopyroxene

Exsolution lamellae of ilmenite, apparently parallel to {001} in clinopyroxene (Fig. 5c), also point to an originally high-Ti clinopyroxene. These ilmenite lamellae further show internal exsolution of hematite, similar to that observed in separate Fe–Ti-oxide grains. Exsolution of ilmenite in clinopyroxene usually indicates decreasing *T* and/or increasing *P* (Garrison & Taylor, 1981; Zhang *et al.*, 2003).

Rutile needles in clinopyroxene and garnet

Coarse-grained clinopyroxene in metasomatized eclogite shows a high density of rutile needles in two crystallographic orientations (Fig. 6l). Needles or rods of rutile in garnet, oriented along crystallographically controlled (111) planes, are observed in some coarse-grained pyroxenite samples (Fig. 6m). They are typically restricted to cores of porphyroblastic garnets. Similar textures have been described from UHP rocks elsewhere, and are considered to be important UHP indicators [see, e.g. Hwang *et al.* (2007) for a more thorough discussion].

According to experiments by Zhang *et al.* (2003), the Ti content of garnet coexisting with clinopyroxene is strongly *P*-dependent, and they inferred that rutile exsolution in clinopyroxene and garnet is a potential indicator of UHP metamorphism at mantle depths.

DISCUSSION

Timing of carbonatite crystallization

The 454·5 ± 1·1 Ma age of internally zoned, prismatic zircons is interpreted to represent the magmatic crystallization age of the carbonatite. Equant, sub-rounded zircons show a slightly younger 451·6 ± 1·7 Ma age. Both of these ages are, within the uncertainty limits, identical to the previously reported U–Pb zircon age of 452·1 ± 1·7 Ma inferred for the peak metamorphic stage of the Tromsø eclogite (Corfu *et al.*, 2003).

Carbonatites at converging plate boundaries

Carbonatites in subduction-zone environments have previously been described from the Koettlitz Glacier area in Antarctica by Cooper *et al.* (1997) and Hagen-Peter & Cottle (2016), and from Mt. Vulture, southern Italy (D'Orazio *et al.*, 2007). Carbonatites in collision zones are described from NW Pakistan (Tilton *et al.*, 1998) and western Sichuan, SW China (Hou *et al.*, 2006). Chakhmouradian *et al.* (2008) described post-orogenic carbonatites from Eden Lake within the Trans-Hudson Orogen, northern Manitoba, Canada. Remobilized marbles with intrusive appearance have also been reported in the same settings (e.g. Liu *et al.*, 2006).

In the area studied here, carbonatite clearly has intrusive relationships to eclogite, pyroxenite and marble (Fig. 3a, b, d and f), and commonly shows K-fenitization of the intruded silicate rocks (Fig. 3a, b and e). Such features are not observed along contacts between marble and silicate rocks (Fig. 3h).

Geochemical parameters, such as whole-rock REE patterns of the Tromsø carbonatite, are clearly different from those in the spatially associated marble or calc-silicate marble (Fig. 8b), suggesting different origins. The overlap in C-isotope ratios (Fig. 9) may indicate a crustal contribution to the Tromsø carbonatite. The isotope ratios of the Tromsø carbonatite are, however, consistent with the relationships observed in many carbonatites worldwide (Bell & Simonetti 2010).

The high $(^{87}Sr/^{86}Sr)_i$ and low $\varepsilon Nd(t)$ of the Tromsø carbonatite (Fig. 10) are, however, different from those in rift and intra-plate settings including Fennoscandian (Kola) carbonatites, but similar to those of some other collision-related (e.g. Tilton *et al.*, 1998; Hou *et al.*, 2006) and subduction-related carbonatites (D'Orazio *et al.*, 2007). The Tromsø carbonatite also falls close to carbonatites with enriched (metasomatized) mantle source (Simonetti *et al.*, 1995; Ying *et al.*, 2004; Rosatelli *et al.*, 2007; Xu *et al.*, 2011). In a broad sense, the enriched-mantle source implies the involvement of subducted and recycled crust. The Sr and Nd isotope composition of the eclogite is interesting because it points to an involvement of continental crustal material, consistent with radiogenic Pb isotopic compositions previously observed in the Tromsø eclogites (Corfu *et al.*, 2003), which points to a provenance from mature crustal or enriched-mantle sources.

Geochemical constraints on the geodynamic setting of the carbonatite

Trace element concentrations can provide important clues about the tectonic setting of carbonatites. Most carbonatites in intraplate settings (e.g. continental rifts) are characterized by high concentrations of LILE (especially Sr and Ba) and high field strength elements (HFSE); the average values for Zr, Nb, Hf and Ta are 256·4, 308·9, 4·3 and 8·9 ppm, respectively (Chakhmouradian, 2006). Subduction- and collision-related carbonatites in off-craton settings have high LILE contents, but much lower Zr, Nb, Hf and Ta. For example, Chakhmouradian *et al.* (2008) reported for the Eden Lake carbonatite the following values (ppm): 47–98 for Zr, 4·0 for Nb, 1·5–2·4 for Hf, and 0·2 for Ta. Values of the same magnitude are reported from the subduction-related carbonatites in Italy, Antarctica, northeastern China (Stoppa & Woolley, 1997; Ying *et al.*, 2004; D'Orazio *et al.*, 2007), and even much lower values from the collision-related carbonatites in southwestern and northern China (Hou *et al.*, 2006; Xu *et al.*, 2010). The Tromsø carbonatite with highly depleted HFSE (Zr = 26–460 ppm, average 114; Nb = 1–31, average 18; Hf = 0–7·7, average 2·5; Ta = 0·5–2·0, average 1·2) has the signature of off-craton carbonatites.

As the HFSE contents of carbonatites are highly variable, the Zr/Nb and Nb/Ta ratios are commonly used to indicate petrogenesis. Average carbonatites (mostly intraplate) have Zr/Nb = 0·8 and Nb/Ta = 35 (Chakhmouradian, 2006), whereas corresponding average ratios for the Tromsø carbonatite are 19 and 18, respectively; that is, significantly different from on-craton carbonatites, but close to the ratios of most subduction- and collision-related carbonatites (Fig. 11). Moreover, the Tromsø and some other off-craton carbonatites have Zr/Nb and Nb/Ta ratios similar to primordial mantle, which is consistent with the origin of primitive carbonate melts according to the genetic model of Chakhmouradian (2006). It is well established that refractory rutile in a subducted slab will retain Nb, thereby increasing Zr/Nb and lowering Nb/Ta in magma generated by partial melting of the slab (Dalton & Blundy, 2000; Foley *et al.*, 2000).

Petrogenesis

The petrogenesis of carbonatites has been debated for several decades. Proposed origins include low-*P* liquid immiscibility from parental nephelinite magmas (e.g. Le Bas, 1987) and generation of primary carbonatite magma by partial melting of carbonated rocks ($\pm H_2O$) of various compositions, including mantle peridotite (e.g. Wallace & Green, 1988; Bailey, 1989), basalt (Dasgupta *et al.*, 2004, 2005; Kiseeva *et al.*, 2012) and pelite (Thomsen & Schmidt, 2008). Another proposed theory is that carbonatites are residual melts of fractionated carbonated nephelinite or melilitite (Gittins, 1989; Gittins & Jago 1998). In a few cases, carbonatites apparently formed by melting of sedimentary carbonates within the crust (Liu *et al.*, 2006).

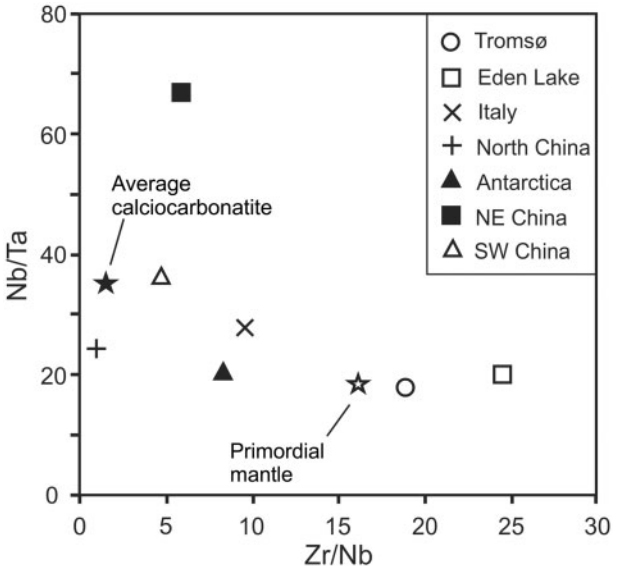

Fig. 11. Nb/Ta vs Zr/Nb diagram for the Tromsø carbonatites, together with carbonatites in collision and subduction settings elsewhere. The black and white stars represent the Nb/Ta and Zr/Nb values for the average calciocarbonatites of Chakhmouradian (2006) and Primordial Mantle of McDonough & Sun (1995), respectively. Data sources: Eden Lake, Chakhmouradian *et al.* (2008); Italy, Stoppa & Woolley (1997) and D'Orazio *et al.* (2007); North China, Xu *et al.* (2010); Antarctica, Hagen-Peter & Cottle (2016); NE China, Ying *et al.* (2004); SW China, Hou *et al.* (2006).

Liquid immiscibility and crystal fractionation are unlikely processes in the Tromsø case as (1) there are no alkaline rocks associated with the carbonatite, and (2) Nb over Zr would have preferentially been partitioned into the carbonatitic melt by either of these processes. The associated marbles can also be ruled out as a source of the carbonatite melt owing to different LILE, REE, HFSE and oxygen isotopic compositions. Mixing of magmatic and crustal carbonate also appear to be unlikely, judging from the contrasting $\delta^{18}O_{SMOW}$ values. The C- and O-isotope signatures (Fig. 9) of the Tromsø carbonatite show some similarities to carbonatites from Greenland, North America and Europe (Bell, 2005). The sharp cross-cutting contact between marble and carbonatite (Fig. 3f) and the absence of melting features in the marbles support this conclusion.

The strongly fractionated REE patterns of the carbonatite indicate that the primary melt formed in the presence of residual garnet. The high concentrations of K, P and Ti in the most pristine carbonatite point toward a source that most probably contained phengite, apatite and a Ti-rich phase.

Based on the geochemical signatures of eclogite and carbonatite in this study, carbonated eclogite was the most likely source of the carbonatite magma. The observed low Nb/Ta ratios and low Nb content of the carbonatite are consistent with melting of an eclogitic source. Experimental evidence (Dalton & Blundy 2000;

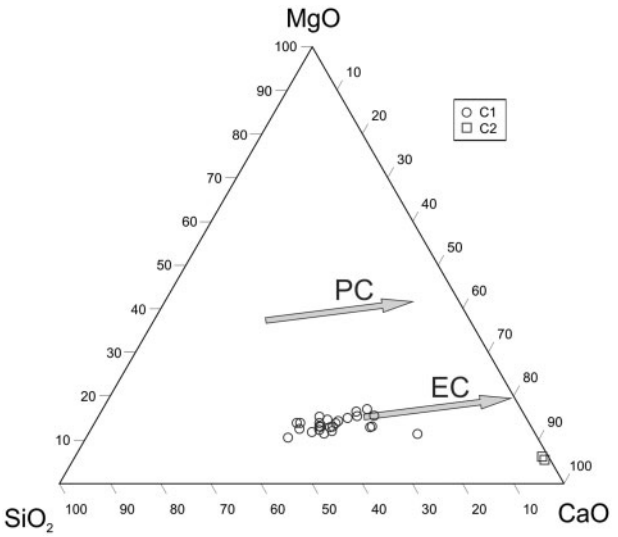

Fig. 12. SiO_2–MgO–CaO diagram showing the compositions of the Tromsø carbonatite. PC, carbonatitic melts in equilibrium with carbonated peridotite (Dalton & Presnall, 1998; Gudfinnsson & Presnall, 2005); EC, carbonatitic melts in equilibrium with carbonated eclogite (Yaxley & Brey, 2004).

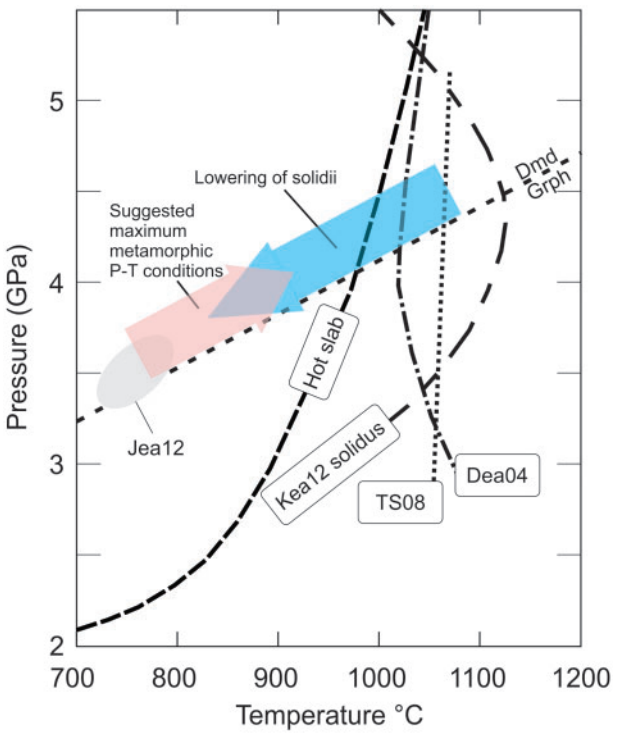

Fig. 13. Summary of *P–T* estimates for eclogite and generation of carbonatitic melt. Jea12: *P–T* conditions of Ky–Phe-bearing eclogite, Tromsø Nappe (Janák *et al.*, 2012). Solidus curves for melting of carbonated eclogite: Dea04, Dasgupta *et al.* (2004); TS08, Thomsen & Schmidt (2008); Kea12, Kiseeva *et al.* (2012). Trajectory for hot slab is from van Keken *et al.* (2002). The transition from graphite to diamond is from Day (2012). The fields marked 'Lowering of solidi' and 'Suggested maximum metamorphic *P–T* conditions' are based on the discussion given in the main text.

Klemme *et al.*, 2002) shows that HFSE-depleted, off-craton carbonatites may be derived by 1–30% partial melting of a rutile-bearing eclogitic source. In this case, the presence of rutile rimmed by titanite in the carbonatite matrix can be interpreted as a reaction between the refractory rutile and a reactive carbonatite melt or fluid. The role of the rutile as the main Nb-bearing refractory phase during partial melting of eclogite is inferred also from the lower Nb abundances in the carbonatite compared with eclogite (1–31 ppm and 7–33 ppm, respectively). Moreover, the Tromsø carbonatite compositions plot in the ternary SiO_2–MgO–CaO diagram (Fig. 12) along the compositional line defined by carbonatite melts in equilibrium with carbonated eclogite (EC) and differ significantly from the line defined by carbonatite melts in equilibrium with carbonated peridotite (PC). This is consistent with experimental data that show more calcic composition of carbonatite melt derived from an 'eclogite' than from a 'peridotite' source (Yaxley & Brey, 2004; Kiseeva *et al.*, 2012). The same source and genetic link of carbonatites and carbonated and metasomatized eclogites is also supported by their position on a single Rb–Sr errorchron (Fig. 7c), whereas no marble or pristine eclogite plot on errorchron.

A summary of the relevant *P–T* conditions for the generation of carbonatite melt is shown in Fig. 13. This model may also explain the apparent genetic link between carbonatite and eclogite.

Melting experiments on nominally anhydrous carbonated eclogite compositions (Dasgupta *et al.*, 2004; Yaxley & Brey, 2004; Thomsen & Schmidt, 2008; Kiseeva *et al.*, 2012) show that the location of the carbonatite solidus varies over a large (1000–1300°C) temperature range at 3–4·5 GPa (see Fig. 13). In the experiments of Dasgupta *et al.* (2004) and Yaxley & Brey (2004), the determined solidi remain hotter than the range of typical subduction geotherms, at least down to the transition zone at 400 km (Dasgupta *et al.*, 2004). According to Dasgupta *et al.* (2004), this suggests that melting-induced release of carbonates from a (dry) subducting crust will not occur at least until the slab reaches the base of the upper mantle.

Experiments also demonstrate that a significant lowering of melting temperatures of carbonated eclogite can be achieved by adding components such as Na_2O (Yaxley & Brey, 2004), H_2O and K_2O (Kiseeva *et al.*, 2012). Brey *et al.* (2009) presented experiments on melting of carbonated peridotite demonstrating lowering of the solidus by addition of H_2O and F to the system. Jago & Gittins (1991) argued that the presence of F could significantly reduce (by 160–290°C) the solidus temperatures of carbonatite magmas. The influence of P_2O_5 on melting of carbonated eclogite is unknown, but it may show a similar effect to that for carbonated peridotite. Baker & Wyllie (1992) demonstrated that P_2O_5 would readily enter carbonate-rich melts, and will probably also contribute to push the solidus toward lower *T*. As the Tromsø carbonatite contains substantial

amounts of phlogopite and fluorapatite, it is reasonable to suggest that the presence of F, P_2O_5, K_2O and H_2O played an important role in lowering the solidus of the source rock (carbonated eclogite) to temperatures experienced in the subducted crust (Fig. 13). The calculated metamorphic *P*–*T* conditions of eclogite (3·5 GPa; 750–800°C) of Ravna & Roux (2006) and Janák *et al.* (2012) may be regarded as minimum values, assuming retrograde diffusion and re-equilibration processes during exhumation.

The presence of Mg–(Fe)-calcite instead of aragonite at such high *P* is unexpected, but HP melting experiments on carbonated eclogite (Kiseeva *et al.*, 2012) have shown that the stable carbonate phase at such conditions is Mg-calcite (82·8–92·3 mol % $CaCO_3$, 2·87–5·27 mol % $FeCO_3$ and 4·59–11·9 mol % $MgCO_3$). For a comparison, the reintegrated carbonate from the Tromsø carbonatite has 77–79 mol % $CaCO_3$, 5 mol % $FeCO_3$ and 12–13 mol % $MgCO_3$ (Broska *et al.*, 2014).

A possible scenario for the generation of the primary carbonatite magma implies deep subduction of continental crust (or continent–ocean transition zone) and partial melting of carbonated eclogite (and eventually other crustal rocks) at mantle depths. This process can be equivalent to the formation of silicate melt in partially melted eclogites (e.g. Skjerlie & Patiño-Douce, 2002) and anatectic migmatites. It is known that subduction and UHP metamorphism of the Tromsø Nappe occurred in the Ordovician (*c.* 450–470 Ma), before closure of the Iapetus ocean and collision between Laurentia and Baltica; however, the detailed paleogeographical situation and tectonic setting is still not understood.

During the subsequent cooling and crystallization of the carbonatite magma, various host rocks were fenitized by K-rich fluids. This process resulted in the formation of glimmerite and phlogopite-rich pyroxenite, and was probably responsible for the locally observed K depletion of the carbonatite. Potassium fenitization has also been reported in the Cargill Complex near Kapuskasing, Ontario (Gittins *et al.*, 1975). The late growth of allanite along interfaces between calcite and silicates is most probably related to autometasomatism by late REE-enriched magmatic fluids.

CONCLUSIONS

The Tromsø carbonatite is a unique natural example of such rocks in a UHP metamorphic terrane. Based on the geochemical signatures, carbonated eclogite was the major source of the carbonatite magma.

Field observations indicate that carbonatite magma intruded the host UHP rocks—eclogite pyroxenite, diamond-bearing gneiss, and marble. Microtextures and mineral compositions suggest that all the primary matrix phases of the carbonatite crystallized simultaneously. The highly reactive carbonatite melt locally metasomatized the host eclogite and pyroxenite.

The *P*–*T* conditions of carbonatite-melt formation are uncertain, but it is likely that carbonatite was generated in the deeply subducted slab of continental crust, at UHP conditions ($P \geq 3{\cdot}5$ GPa and $T \geq 750$°C). As melting temperatures of dry carbonated eclogite are too high for typical subduction-zone geotherms, the presence of the additional components H_2O, K_2O, P_2O_5 and F (in phlogopite and fluorapatite) may imply a substantial lowering of the solidus of the source rock, and a more or less *in situ* generation of the carbonatite melt is suggested.

ACKNOWLEDGEMENTS

We are grateful for the thorough and constructive reviews of Graham Hagen-Peter and Greg Yaxley.

FUNDING

Grants covering analytical expenses (to E.K.R.) were kindly supported by the Norwegian Academy of Science through 'Nansenfondet og de dermed forbundne fond'. Stable isotope analyses were funded by US NSF grant EAR-0711091. D.Z. acknowledges Russian Government grant 0231-2015-0009, and M.J. acknowledges the Slovak Research and Development Agency (project APVV-14-0278).

SUPPLEMENTARY DATA

Supplementary data for this paper are available at *Journal of Petrology* online.

REFERENCES

Anovitz, L. M. & Essene, E. J. (1987). Phase equilibria in the system $CaCO_3$–$MgCO_3$–$FeCO_3$. *Journal of Petrology* **28**, 389–414.

Bailey, D. K. (1989). Carbonate melt from the mantle in the volcanoes of south-east Zambia. *Nature* **338**, 415–418.

Baker, M. B. & Wyllie, P. J. (1992). High-pressure apatite solubility in carbonate-rich liquids: implications for mantle metasomatism. *Geochimica et Cosmochimica Acta* **56**, 3409–3422.

Bell, K. (2005). Carbonatites. In: Selley, R. C., Cocks, L. R. M. & Plimer, I. R. (eds) *Encyclopedia of Geology*. Elsevier, pp. 217–233.

Bell, K. & Simonetti, A. (2010). Source of parental melts to carbonatites—critical isotopic constraints. *Mineralogy and Petrology* **98**, 77–89.

Bindi, L., Safonov, O. G., Yapaskurt, V. O., Perchuk, L. L. & Menchetti, S. (2003). Ultrapotassic clinopyroxene from the Kumdy-Kol microdiamond mine, Kokchetav Complex, Kazakhstan: occurrence, composition and crystal-chemical characterization. *American Mineralogist* **88**, 464–468.

Bouvier, A., Vervoort, J. D. & Patchett, P. J. (2008). The Lu–Hf and Sm–Nd isotopic composition of CHUR: constraints from unequilibrated chondrites and implications for the bulk composition of terrestrial planets. *Earth and Planetary Science Letters* **273**, 48–57.

Bozhilov, K. N., Xu, Z., Dobrzhinetskaya, L. F., Jin, Z.-M. & Green, H. W. (2009). Cation-deficient phlogopitic mica exsolution in diopside from garnet peridotite in SuLu, China. *Lithos* **109**, 304–313.

Brey, G. P., Bulatov, V. K. & Girnis, A. V. (2009). Influence of water and fluorine on melting of carbonated peridotite at 6 and 10 GPa. *Lithos* **112**, 249–259.

Bromiley, G. D., Keppler, H., McCammon, C., Bromiley, F. A. & Jacobsen, S. D. (2004). Hydrogen solubility and speciation in natural, gem-quality chromian diopside. *American Mineralogist* **89**, 941–949.

Broska, I., Ravna, E. J. K., Vojtko, P., Janák, M., Konecny, P., Pentrak, M., Bacik, P., Luptakova, J. & Kullerud, K. (2014). Oriented inclusions in apatite in a post-UHP fluid-mediated regime (Tromsø Nappe, Norway). *European Journal of Mineralogy* **26**, 623–634.

Castelli, D., Rolfo, F., Groppo, C. & Compagnoni, R. (2007). Impure marbles from the UHP Brossasco–Isasca Unit (Dora–Maira Massif, western Alps): evidence for Alpine equilibration in the diamond stability field and evaluation of the $X(CO_2)$ fluid evolution. *Journal of Metamorphic Geology* **25**, 587–603.

Cazes, J. (2005). *Ewing's Analytical Instrumentation Handbook*, 3rd edn. Marcel Dekker, 1037 pp.

Chakhmouradian, A. R. (2006). High-field-strength elements in carbonatitic rocks: geochemistry, crystal chemistry and significance for constraining the sources of carbonatites. *Chemical Geology* **235**, 138–160.

Chakhmouradian, A. R., Mumin, A. H., Demény, A. & Elliott, B. (2008). Postorogenic carbonatites at Eden Lake, Trans-Hudson Orogen (northern Manitoba, Canada): geological setting, mineralogy and geochemistry. *Lithos* **103**, 503–526.

Chakhmouradian, A. R., Reguir, E. P. & Zaitsev, A. N. (2016). Calcite and dolomite in intrusive carbonatites. I. Textural variations. *Mineralogy and Petrology* **110**, 333–360.

Coleman, R. G. (1961). Jadeite deposits of the Clear Creek Area, New Idria District, San Benito County, California. *Journal of Petrology* **2**, 209–247.

Cooper, A. F., Worley, B. A., Armstrong, R. A. & Price, R. C. (1997). Synorogenic alkaline and carbonatite magmatism in the Transantarctic Mountains of South Victoria Land, Antarctica. In: Ricci, C. A. (ed.) *The Antarctic Region: Geological Evolution and Processes. Proceedings of the VII International Symposium on Antarctic Earth Sciences, Siena 1995. Siena*. Terra Antarctica Publication. pp. 245–252.

Corfu, F. (2004). U–Pb age, setting, and tectonic significance of the anorthosite–mangerite–charnockite–granite suite, Lofoten–Vesterålen, Norway. *Journal of Petrology* **45**, 1799–1819.

Corfu, F., Ravna, E. J. K. & Kullerud, K. (2003). A late Ordovician U–Pb age for the Tromsø Nappe eclogites, uppermost allochthon of the Scandinavian Caledonides. *Contributions to Mineralogy and Petrology* **145**, 502–513.

Dalton, J. & Blundy, J. (2000). Carbonatites from recycled eclogites. *Journal of Conference Abstracts* **5**, 330.

Dalton, J. A. & Presnall, D. C. (1998). The continuum of primary carbonatitic–kimberlitic melt compositions in equilibrium with lherzolite: data from the system $CaO–MgO–Al_2O_3–SiO_2–CO_2$ at 6 GPa. *Journal of Petrology* **39**, 1953–1964.

Dasgupta, R., Hirschmann, M. M. & Withers, A. C. (2004). Deep global cycling of carbon constrained by the solidus of anhydrous carbonated eclogite under upper mantle conditions. *Earth and Planetary Science Letters* **227**, 73–85.

Dasgupta, R., Hirschmann, M. M. & Dellas, N. (2005). The effect of bulk compositions on the solidus of carbonated eclogite from partial melting experiments at 3 GPa. *Contributions to Mineralogy and Petrology* **149**, 288–305.

Day, H. (2012). A revised diamond–graphite transition curve. *American Mineralogist* **97**, 52–62.

Deines, P. (1989). Stable isotope variations in carbonatites. In: Bell, K. (ed.) *Carbonatites: Genesis and Evolution*. Unwin Hyman, pp. 301–359.

Dobrzhinetskaya, L. F., Wirth, R., Rhede, D., Liu, Z. & Green, H. W. (2009). Phlogopite and quartz lamellae in diamond-bearing diopside from marbles of the Kokchetav massif, Kazakhstan: exsolution or replacement reaction? *Journal of Metamorphic Geology* **27**, 607–620.

D'Orazio, M., Innocenti, F., Tonarini, S. & Doglioni, C. (2007). Carbonatites in a subduction system: the Pleistocene alvikites from Mt. Vulture (southern Italy). *Lithos* **98**, 313–334.

Ferrando, S., Proyer, A., Castelli, D., Compagnoni, R. & Frezzotti, M. L. (2011). Complex metamorphic evolution in metamorphic carbonates: application of cathodoluminiscence to impure UHP calcite–dolomite marbles from the Dora–Maira massif (Western Alps). In: Lexa, O. (ed.) *Abstract Volume of the 9th International Eclogite Conference, Mariánské Lázně 6.-9.8. 2011, Czech Republic*. p. 19.

Foley, S. F., Barth, M. G. & Jenner, G. A. (2000). Rutile/melt partition coefficients for trace elements and an assessment of the influence of rutile on the trace element characteristics of subduction zone magmas. *Geochimica et Cosmochimica Acta* **64**, 933–938.

Garrison, J. R. & Taylor, L. A. (1981). Petrogenesis of pyroxene–oxide intergrowths from kimberlite and cumulate rocks: coprecipitation or exsolution? *American Mineralogist* **66**, 723–740.

Gittins, J. (1989). The origin and evolution of carbonatite magmas. In: Bell. K. (ed.) *Carbonatites: Genesis and Evolution*. Unwin Hyman, pp. 580–600.

Gittins, J. & Jago, B. C. (1998). Differentiation of natrocarbonatite magma at Oldoinyo Lengai volcano, Tanzania. *Mineralogical Magazine* **62**, 759–768.

Gittins, J., Allen, C. R. & Cooper, A. F. (1975). Phlogopitization of pyroxenite—its bearing on composition of carbonatite magmas. *Geological Magazine* **112**, 503–507.

Goldstein, S. J. & Jacobsen, S. B. (1988). Nd and Sr isotopic systematics of river water suspended material: implications for crystal evolution. *Earth and Planetary Science Letters* **87**, 249–265.

Green, D. H. & Wallace, M. E. (1988). Mantle metasomatism by ephemeral carbonatite melts. *Nature* **336**, 459–462.

Gudfinnsson, G. H. & Presnall, D. C. (2005). Continuous gradations among primary carbonatitic, kimberlitic, melilititic, basaltic, picritic, and komatiitic melts in equilibrium with garnet lherzolite at 3–8 GPa. *Journal of Petrology* **46**, 1645–1659.

Hagen-Peter, G. & Cottle, J. M. (2016). Synchronous alkaline and subalkaline magmatism during the late Neoproterozoic–early Paleozoic Ross orogeny, Antarctica: insights into magmatic sources and processes within a continental arc. *Lithos* **262**, 677–698.

Harlow, G. E. (1997). K in clinopyroxene at high pressure and temperature. *American Mineralogist* **82**, 259–269.

Hou, Z., Tian, S., Yuan, Z., Xie, Y., Yin, S., Yi, L., Fei, H. & Yang, Z. (2006). The Himalayan collision zone carbonatites in western Sichuan, SW China: petrogenesis, mantle source and tectonic implication. *Earth and Planetary Science Letters* **244**, 234–250.

Hwang, S. L., Shen, P., Chu, H.-T., Yui, T. F., Liou, J. G., Sobolev, N. V., Zhang, R. Y., Shatsky, V. S. & Zayachkovsky, A. A. (2004). Kokchetavite: a new potassium-feldspar polymorph from the Kokchetav ultrahigh-pressure terrane. *Contributions to Mineralogy and Petrology* **148**, 380–389.

Hwang, S. L., Yui, T. F., Chu, H. T., Shen, P., Schertl, H. P., Zhang, R. Y. & Liou, J. G. (2007). On the origin of oriented

rutile needles in garnet from UHP eclogites. *Journal of Metamorphic Geology* **25**, 349–362.
Jago, B. C. & Gittins, J. (1991). The role of fluorine in carbonatite magma evolution. *Nature* **349**, 56–58.
Janák, M., Ravna, E. J. K. & Kullerud, K. (2012). Constraining peak *P–T* conditions in UHP eclogites: calculated phase equilibria in kyanite- and phengite-bearing eclogite of the Tromsø Nappe, Norway. *Journal of Metamorphic Geology* **30**, 377–396.
Janák, M., Ravna, E. J. K., Kullerud, K., Yoshida, K., Milovsky, R. & Hirajima, T. (2013). Discovery of diamond in the Tromsø Nappe, Scandinavian Caledonides (N. Norway). *Journal of Metamorphic Geology* **31**, 691–703.
Janák, M., Uher, P., Ravna, E. K., Kullerud, K. & Vrabec, M. (2015). Chromium-rich kyanite, magnesiostaurolite and corundum in ultrahigh-pressure eclogites (examples from Pohorje Mountains, Slovenia and Tromsø Nappe, Norway). *European Journal of Mineralogy* **27**, 377–392.
Katayama, I., Ohta, M. & Ogasawara, Y. (2002). Mineral inclusions in zircon from diamond-bearing marble in the Kokchetav massif, northern Kazakhstan. *European Journal of Mineralogy* **14**, 1103–1108.
Keller, J. & Hoefs, J. (1995). Stable isotope characteristics of recent natrocarbonatites from Oldoinyo Lengai. In: Bell, K. & Keller, J. (eds) *Carbonatite Volcanism: Oldoinyo Lengai and the Petrogenesis of Natrocarbonatites*. Springer, pp. 113–123.
Kiseeva, E. S., Yaxley, G. M., Hermann, J., Litasov, K. D., Rosenthal, A. & Kamenetsky, V. S. (2012). An experimental study of carbonated eclogite at 3·5–5·5 GPa—implications for silicate and carbonate metasomatism in the cratonic mantle. *Journal of Petrology* **53**, 727–759.
Klemme, S., Blundy, J. D. & Wood, B. J. (2002). Experimental constraints on major and trace element partitioning during partial melting of eclogite. *Geochimica et Cosmochimica Acta* **66**, 3109–3123.
Korsakov, A. V. & Hermann, J. (2006). Silicate and carbonate melt inclusions associated with diamonds in deeply subducted carbonate rocks. *Earth and Planetary Science Letters* **241**, 104–118.
Kretz, R. (1983). Symbols for rock-forming minerals. *American Mineralogist* **68**, 277–279.
Krogh, E. J., Andresen, A., Bryhni, I., Broks, T. M. & Kristensen, S. E. (1990). Eclogites and polyphase *P–T* cycling in the Caledonian uppermost allochthon in Troms, northern Norway. *Journal of Metamorphic Geology* **8**, 289–309.
Le Bas, M. J. (1987). Nephelinites and carbonatites. In: Fitton, J. G., & Upton, B. G. J. (eds) *Alkaline Igneous Rocks. Geological Society, London, Special Publications* **30**, 85–94.
Le Bas, M. J. (1999). Sövite and alvikite: two chemically distinct calciocarbonatites C1 and C2. *South Africa Journal of Geology* **102**, 109–121.
Le Bas, M. J., Mian, J. & Rex, D. C. (1987). Age and nature of carbonatite emplacement in North Pakistan. *Geologische Rundschau* **76**, 317–321.
Le Maitre, R. W. (ed.) (2002). *Igneous Rocks: A Classification and Glossary of Terms*. Cambridge University Press, 236 pp.
Lindsley, D. H. (1973). Delimitation of the hematite–ilmenite miscibility gap. *Geological Society of America Bulletin* **84**, 657–662.
Liu, Y., Berner, Z., Massonne, H.-J. & Zhong, D. (2006). Carbonatite-like dykes from the eastern Himalayan syntaxis: geochemical, isotopic, and petrogenetic evidence for melting of metasedimentary carbonate rocks within the orogenic crust. *Journal of Asian Earth Sciences* **26**, 105–120.
Locke, J. & Butler, J. (1993). Characterisation of rock formations for the improved calibration of nuclear logging tools. *Transactions of the fifteenth European Formation Evaluation Symposium, Stavanger, Norway, May 5-7, 1993*, Paper R 1-22.
Luth, R. W. (1997). Experimental study of the system phlogopite–diopside from 3·5 to 17 GPa. *American Mineralogist* **82**, 1198–1209.
Massonne, H.-J. (2011). Phase relations of siliceous marbles at ultrahigh pressure based on thermodynamic calculations: examples from the Kokchetav Massif, Kazakhstan and the Sulu terrane, China. *Geological Journal* **46**, 114–125.
McDonough, W. F. & Sun, S. (1995). The composition of the Earth. *Chemical Geology* **120**, 223–253.
Morimoto, N., Fabries, J., Ferguson, A. K., Ginzburg, I. V., Ross, M., Seifert, F. A. & Zussman, J. (1989). Nomenclature of pyroxenes. *Canadian Mineralogist* **27**, 143–156.
Ogasawara, Y., Fukasawa, K. & Maruyama, S. (2002). Coesite exsolution from supersilicic titanite in UHP marble from the Kokchetav Massif, northern Kazakhstan. *American Mineralogist* **87**, 454–461.
Palme, H. & O'Neill, H. S. C. (2004). Cosmochemical estimates of mantle composition. In: Holland, H. D. & Turekian, K. K. (eds) *Treatise on Geochemistry*, Vol. **2**. Elsevier, pp. 1–38.
Proyer, A., Mposkos, E., Baziotis, I. & Hoinkes, G. (2008). Tracing high-pressure metamorphism in marbles: phase relations in high-grade aluminous calcite–dolomite marbles from the Greek Rhodope massif in the system $CaO–MgO–Al_2O_3–SiO_2–CO_2$ and indications of prior aragonite. *Lithos* **104**, 119–130.
Proyer, A., Rolfo, F., Castelli, D. & Compagnoni, R. (2011a). Diffusion-controlled reaction textures in an impure calcite marble from Dabie Shan. In: Lexa, O. (ed.) *Abstract Volume of the 9th International Eclogite Conference, Mariánské Láznè 6.-9.8. 2011, Czech Republic*, p. 56.
Proyer, A., Rolfo, F., Zhu, Y.-F., Castelli, D. & Compagnoni, R. (2011b). Two impure dolomitic marbles with magnesite and calcite from the Dabie–Sulu UHP belt: reaction history and implications. In: Lexa, O. (ed.) *Abstract Volume of the 9th International Eclogite Conference, Mariánské Lázně 6.-9.8. 2011, Czech Republic*, p. 56–57.
Ravna, E. J. K. & Roux, M. R. M. (2006). Metamorphic evolution of the Tønsvika eclogite, Tromsø Nappe—evidence for a new UHPM province in the Scandinavian Caledonides. *International Geology Review* **48**, 861–881.
Ravna, E. J. K., Kullerud, K. & Ellingsen, E. (2006). Prograde garnet-bearing ultramafic rocks from the Tromsø Nappe, northern Scandinavian Caledonides. *Lithos* **92**, 336–356.
Roberts, D. & Gee, D. G. (1985). An introduction to the structure of the Scandinavian Caledonides. In: Gee, D. G. & Sturt, B. A. (eds) *The Caledonian Orogen—Scandinavia and Related Areas*. John Wiley, pp. 56–68.
Rosatelli, G., Wall, F. & Stoppa, F. (2007). Calcio-carbonatite melts and metasomatism in the mantle beneath Mt. Vulture (Southern Italy). *Lithos* **99**, 229–248.
Rukhlov, A. S., Bell, K. & Amelin, Y. (2015). Carbonatites, isotopes and evolution of the subcontinental mantle: an overview. In: Simandl, G. J. & Neetz, M. (eds) *Symposium on Strategic and Critical Materials Proceedings, November 13–14, 2015, Victoria, British Columbia. British Columbia Ministry of Energy and Mines, British Columbia Geological Survey Paper* **2015**, 39–64.
Schertl, H.-P. & Okay, A. I. (1994). A coesite inclusion in dolomite in Dabie Shan, China: petrological and rheological significance. *European Journal of Mineralogy* **6**, 995–1000.
Simonetti, A., Bell, K. & Viladkar, S. G. (1995). Isotopic data from the Amba Dongar carbonatite complex, west–central India: evidence for an enriched mantle source. *Chemical Geology* **122**, 185–198.

Skjerlie, K. P. & Patiño Douce, A. E. (2002). The fluid-absent partial melting of a zoisite-bearing quartz eclogite from 1·0 to 3·2 GPa; implications for melting in thickened continental crust and for subduction zone processes. *Journal of Petrology* **43**, 291–314.

Sklyarov, E. V., Fedorovsky, V. S., Kotov, A. B., Lavrenchuk, A. V., Mazukabzov, A. M., Levitsky, V. I., Sal'nikova, E. B., Starikova, A. E., Yakoleva, S. Z., Anisimova, I. V. & Fedoseenko, A. M. (2009). Carbonatites in collisional settings and pseudo-carbonatites of the Early Paleozoic Ol'khon collisional system. *Russian Geology and Geophysics* **50**, 1091–1106.

Stacey, J. S. & Kramers, J. D. (1975). Approximation of terrestrial lead isotope evolution by a two-stage model. *Earth and Planetary Science Letters* **34**, 207–226.

Stevenson, J. A. (2005). High pressure partial melting of eclogite and garnet amphibolite rocks during decompression and heating, Tromsö Nappe, Norway. *EOS Transactions American Geophysical Union* **85**, Abstract T23C-03.

Steiger, R. H. & Jäger, E. (1977). Subcommission on geochronology: convention on the use of decay constants in geo- and cosmochronology. *Earth and Planetary Science Letters* **36**, 359–362.

Stoppa, F. & Woolley, A. R. (1997). The Italian carbonatites: field occurrence, petrology and regional significance. *Mineralogy and Petrology* **59**, 43–67.

Taylor, H. P., Jr, Frechen, J. & Degens, E. T. (1967). Oxygen and carbon isotope studies of carbonatites from the Laacher See District, West Germany and the Alnö District, Sweden. *Geochimica et Cosmochimica Acta* **31**, 407–430.

Thomsen, T. & Schmidt, M. W. (2008). Melting of carbonated pelites at 2·5–5·0 GPa, silicate–carbonatite liquid immiscibility, and potassium–carbon metasomatism of the mantle. *Earth and Planetary Science Letters* **267**, 17–31.

Tilton, G. R., Bryge, J. G. & Mateen, A. (1998). Pb–Sr–Nd isotope data from 30 and 300 Ma collision zone carbonatites in Northwest Pakistan. *Journal of Petrology* **39**, 1865–1874.

van Keken, P. E., Kiefer, B. & Peacock, S. M. (2002). High resolution models of subduction zones: implications for mineral dehydration reactions and the transport of water into the deep mantle. *Geochemistry, Geophysics, Geosystems* **3**, doi:10.1029/2001GC000256.

Wallace, M. E. & Green, D. H. (1988). An experimental determination of primary carbonatite magma composition. *Nature* **335**, 343–346.

Xu, C., Kynicky, J., Chakhmouradian, A. R., Qi, L. & Song, W. (2010). A unique Mo deposit associated with carbonatites in the Qinling orogenic belt, central China. *Lithos* **118**, 50–60.

Xu, C., Taylor, R. N., Kynicky, J., Chakhmouradian, A. R., Song, W. & Wang, L. (2011). The origin of enriched mantle beneath North China block: evidence from young carbonatites. *Lithos* **127**, 1–9.

Yaxley, G. M. & Brey, G. P. (2004). Phase relations of carbonate-bearing eclogite assemblages from 2·5 to 5·5 GPa: implications for petrogenesis of carbonatites. *Contributions to Mineralogy and Petrology* **146**, 606–619.

Ying, J., Zhou, X. & Zhang, H. (2004). Geochemical and isotopic investigation of the Laiwu–Zibo carbonatites from western Shandong Province, China, and implications for their petrogenesis and enriched mantle source. *Lithos* **75**, 413–426.

Zhang, R. Y., Liou, J. G., Ernst, W. G., Coleman, R. G., Sobolev, N. V. & Shatsky, V. S. (1997). Metamorphic evolution of diamond-bearing and associated rocks from the Kokchetav massif, northern Kazakhstan. *Journal Metamorphic Geology* **15**, 479–496.

Zhang, R. Y., Zhai, S. M., Fei, Y. W. & Liou, J. G. (2003). Titanium solubility in coexisting garnet and clinopyroxene at very high pressure: the significance of exsolved rutile in garnet. *Earth and Planetary Science Letters* **216**, 591–601.